Universitatea Politehnica București

Școala Doctorală de Electronică, Telecomunicații și Tehnologia Informației din București (SD-ETTI-B) România

Universitatea de Medicină și Farmacie „Carol Davila" București

Școala Doctorală a Universității de Medicină și Farmacie „Carol Davila " București

Ph.D. co-supervision agreement no. 232/09.01.2017 and no. 6372/06.03.2017

No. Decision 628 din 14.12.2020

Ph.D. Thesis Summary

RESEARCH IN THYROID PATHOLOGY USING UNCONVENTIONAL HIGH-RESOLUTION LASER BEAM TECHNIQUES

Ph.D. student: Med. Lucian-George EFTIMIE

DOCTORAL COMMISSION

Președinte	**Prof. Dr. Ing. Bogdan IONESCU**	de la	**Universitatea Politehnica București**
Conducător de doctorat	**Prof .Dr. Ing. Gheorghe STANCIU**	de la	**Universitatea Politehnica București**
Coordonator cotutelă	**Prof.Dr. Med. Maria SAJIN**	de la	**Universitatea de Medicină și Farmacie „Carol Davila" București**
Referent	**Prof. Dr. Ing. Gheorghe BREZEANU**	de la	**Universitatea Politehnica București**
Referent	**Prof. Dr. Med. Mariana COSTACHE**	de la	**Universitatea de Medicină și Farmacie „Carol Davila" București**

BUCHAREST

2020

Thanks

The content of the Ph.D. thesis

Chapter 1 - Introduction

The World Health Organization announces cancer as one of the leading causes of morbidity and mortality, being the second leading cause of death in the world after cardiovascular disease. Thyroid cancer accounts for 92% of all endocrine neoplasms. Cancer mortality can be reduced if cases are detected and treated early.

The clinical and imaging diagnosis of malignancy is confirmed or refuted in the departments of pathology, histopathology and cytopathology being the main tools used in the diagnosis of cancer. The histopathological diagnosis of thyroid nodules on paraffin sections of suspicious thyroid tissue is the gold standard in differentiating benign from malignant lesions.

Due to the increasing incidence or overdiagnosis of thyroid carcinomas both worldwide and in Romania, the main purpose of this thesis is to find a potential new helpful method, complementary to traditional optical microscopic examination in accurately and rapidly diagnosing thyroid malignancies, just by studying their capsule.

1.1 The field of the Ph.D. thesis

A complementary method for diagnostic purposes that could be used in the pathology of encapsulated thyroid neoplasms is the use of unconventional high-resolution laser beam techniques.

Any experiment of this type can be performed only through an interdisciplinary collaboration between a University of Biomedical Sciences - University of Medicine and Pharmacy Bucharest (a pathologist who analyzes biological samples from a medical point of view and who works in a Department of Pathology of a hospital - for example the Central Military Emergency University Hospital "Dr. Carol Davila", Bucharest) and a Technical University - Polytechnic University of Bucharest (with high performance equipment and researchers' knowledge of alternative methods of quantitative microscopy and image processing - for example the Center for Microscopy, Microanalysis and Information Processing). This collaboration thus corresponds to the need for an accurate and rapid diagnosis in a difficult medical case that can be faced by a pathologist (medical idea), where you will find the important contribution of technology, state-of-the-art equipment and training of a research engineer (the idea of new imaging methods, conceived so far, on biological or non-biological structures) and led to the very good results of the research studies exclusively on biological samples.

1.2. The purpose of the PhD thesis

Finding a potential new helpful method, complementary to the traditional optical microscopic examination in accurately and quickly diagnosing thyroid malignant nodules, this consists in studying the distribution of collagen fibers in the fibrous capsule of pathological thyroid nodules through laser scanning microscopy.

The research topic addresses a complex topic regarding the elaboration of a more accurate differential diagnosis of encapsulated thyroid nodules (benign and malignant), being known that the pathologist is sometimes struck by the lack of total visualization under the light microscope adjacent thyroid indemnity.

I thought it would be necessary to visualize by a microscopic method the capsule surrounding the suspicious thyroid tumor nodule, in its entirety, to discover a possible malignant transformation or a capsular change that cannot be detected by classical methods.

Thus, we aimed to identify an answer to the question of whether malignant nodules could be differentiated from benign ones, visualizing only the distribution and structural changes of collagen in their capsule, using optical microscopy techniques, especially laser scanning microscopy.

1.3. The content of the Ph.D. thesis

In this paper I aimed to observe the distribution of collagen in the structure of the capsule that delimits: thyroid adenomas (follicular adenoma) and thyroid carcinomas (papillary thyroid carcinoma) apparently encapsulated, using optical microscopy techniques, especially laser scanning microscopy.

Until now, no such research has been performed on the capsular collagen of pathological thyroid nodules.

We resorted to laser scanning microscopy imaging, made with the equipment of the Center for Microscopy, Microanalysis and Information Processing at the Polytechnic University of Bucharest, namely: confocal scanning laser microscopy (CLSM), microscopy based on two-photon excitation fluorescence (TPEF) and second harmonic generation (SHG) microscopy which has proven to be the most useful in this research.

Motivation: because the thyroid capsule is made of collagen, and SHG imaging can be used only in materials that do not have a center of symmetry, such as collagen fibers, we considered that laser scanning microscopy and especially microscopy based on the second harmonics generation could differentiate malignant nodules from benign thyroid ones by highlighting the distribution and structural changes of collagen in their capsule.

Chapter 2 – Current state of the field regarding the study of thyroid pathology

2.1. Embryology, anatomy and histology of the thyroid gland

2.1.1. Embryology of the thyroid gland

The primordium of the thyroid gland appears in Weeks 3-4 of the gestational development of the embryo, at the base of the primitive pharynx, in the foramen cecum. In the following weeks of gestation, it descends from the base of the tongue to the base of the neck, passing in front of the hyoid bone, continues its development, with lateral expansion and the formation of thyroid lobes in the 7th week of gestation. In week 14 of gestation, mature thyroid follicles with colloidal secretion in the lumen can be observed.

2.1.2. Anatomy of the thyroid gland

The thyroid is an endocrine gland, located at the base of the anterior face of the neck, weighing 25-30 grams, having the shape of the letter "H" (butterfly), consisting of two lobes, symmetrical laterally, joined by an isthmus. It is superficially located and easily accessible for inspection and palpation.

2.1.3. Histology of the thyroid gland

The thyroid gland is covered by a fine sclerotic capsule that sends inward fibrous septa that divide the parenchyma into lobules (thyromeres), the thyroid parenchyma being composed mainly of two cell types: parafollicular cells C (secretes calcitonin) and thyroid cells (makeup thyroid follicles), and the structural and functional unit of the thyroid is represented by the thyroid follicle.

2.1.4. Thyroid gland function

The thyroid is responsible for the synthesis and secretion of thyroid hormones - T3, T4, synthesized by follicular cells under the pituitary (TSH), and hypothalamic (TRH). They regulate metabolism, increase protein synthesis in all tissues of the body, increase oxygen consumption and play a crucial role in the development of the body and the normal maturation of the central and peripheral nervous system. The secondary function of the thyroid is represented by the synthesis of calcitonin by C cells, calcitonin being a hormone involved in regulating the plasma level of calcium.

2.2. Histopathological aspects of the thyroid gland

According to the World Health Organization (WHO) - (WHO Classification of Thyroid Gland Tumors, 2017) [14], thyroid tumors fall into three categories: benign tumors (e.g. follicular adenoma), borderline tumors, (borderline, with uncertain behavior - for example, noninvasive thyroid follicular neoplasm with papillary-like nuclei (NIFTP)) and malignant tumors (e.g. papillary thyroid carcinoma). Although most benign tumors cannot be life-threatening, many types of benign tumors have the potential to become cancerous (malignant) through a process known as tumor progression or malignant transformation [6].

2.3. Exploring methods of the thyroid gland

The thyroid gland can be explored by a series of noninvasive methods (anamnesis and clinical examination, thyroid ultrasound, elastography, computed tomography, magnetic resonance imaging, thyroid scintigraphy), minimally invasive (fine needle aspiration under ultrasonographic guidance, followed by examination cytopathological), or by histopathological examination of resected intraoperative or postoperative biological samples.

Chapter 3 – Materials and methods used for the study of the pathology of thyroid nodules

The investigation methods used on the biological samples were: optical microscopy, CLSM), TPEF imaging, and SHG imaging.

Optical microscopy is a technology that allows obtaining details of size and shape, but when structural information of the analyzed specimen is required, the characteristics of this technique are exceeded. The main limitation of optical microscopy is that it gives an image of a sample volume CLSM and multi-photon microscopy brings an improvement in both spatial and axial resolution limits.

CLSM is a scanning microscopy technique that involves the existence of a laser source (coherent light source) in contrast to an incoherent light source as in the case of optical microscopy. The principle of confocal laser scanning microscopy is illustrated in Figure 4.57.
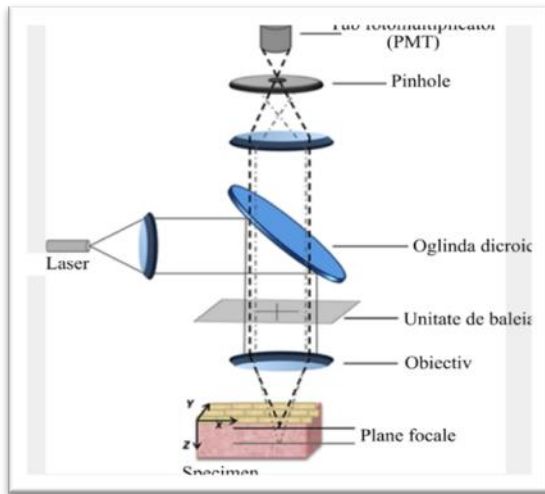
Figura 4.57. Schematic representation of the principle of CLSM

TPEF microscopy is a fluorescence-based imaging technique that allows the image of a tissue to be obtained up to about one millimeter in-depth due to low absorption and much lower excitation light scattering, due to the use of radiation with long wavelengths (infrared) and which has recently been applied in preclinical studies [7].

TPE and SHG imaging techniques offer intrinsic 3D sectioning capabilities with excellent axial resolution. This property allows the optical sectioning of biological tissues with low phototoxicity outside the focal plane [21]. There is a possibility that the radiation produced by TPEF and SHG may be collected forward or backward. A schematic representation of a laser scanning microscope based on TPEF and SHG in Figure 4.76.
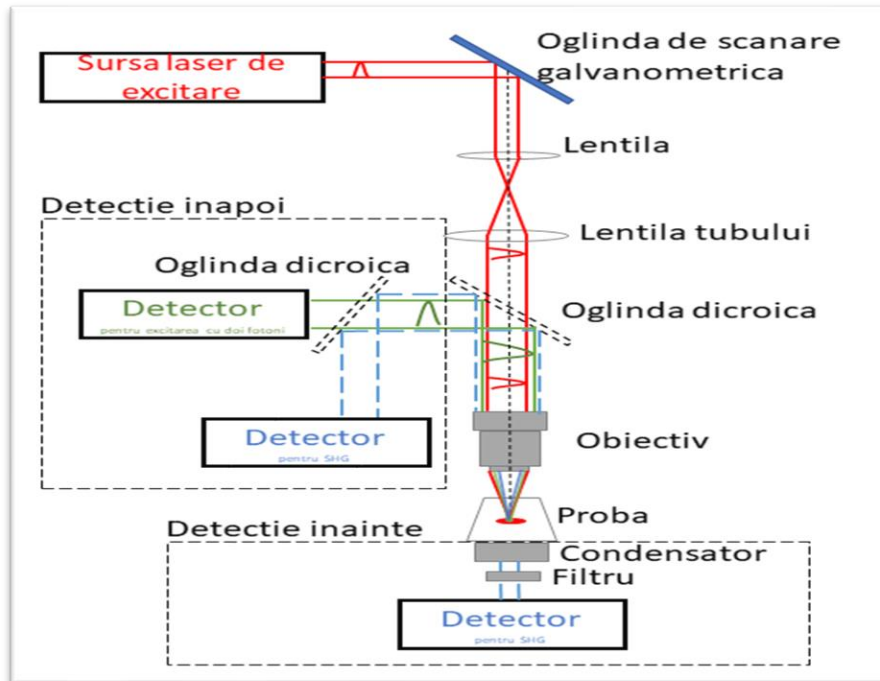
Fig. 4.76. Schematic representation of a laser scanning microscope with 3 simultaneous channels: one of TPEF and two of SHG (one generated forward and one generated backward) [18].

Thus a laser scanning microscope or a confocal microscope can be easily modified to achieve imaging based on nonlinear optical effects.

The material (samples used) for the study of thyroid nodule pathology was collected from histopathologically diagnosed patients after surgery (Central Military Emergency University Hospital "Dr. Carol Davila" Bucharest) for various diseases in the field of thyroid pathology.

Fragments were taken from all macroscopically identified lesions in surgical pieces, as far as possible with the inclusion in the same fragment of both tissues with the pathological and normal macroscopic appearance and their processing according to the standard protocol of the Pathological Anatomy Service of the Military Emergency University Hospital. Central "Dr. Carol Davila "Bucharest, followed by the elaboration of the histopathological diagnosis under the optical microscope.

The tissue fragments selected for research were fixed in aqueous solution, buffered with 10% formaldehyde, incorporated into paraffin, with paraffin block sections of 4-5 microns thick, which were then stretched on slides. Two sections of tissue were consecutively cut from the same block of paraffin: one was stained with Hematoxylin & Eosin and the second was not stained (kept for TPEF and SHG).

Chapter 4 – Experimental results

4.1 Classical Optical Microscopy - Histopathological diagnosis

This chapter presents the thyroid tissue sections investigated by classical light microscopy, stained with standard Hematoxylin & Eosin staining to develop a histopathological diagnosis of benign nodule-follicular adenoma (figure 4.6) or malignant nodule - thyroid papillary carcinoma (figure 4.5), and for difficult cases immunohistochemical tests were performed to confirm the diagnosis, to make a differential diagnosis with other histopathological types of tumor proliferation and to determine tumor histogenesis.
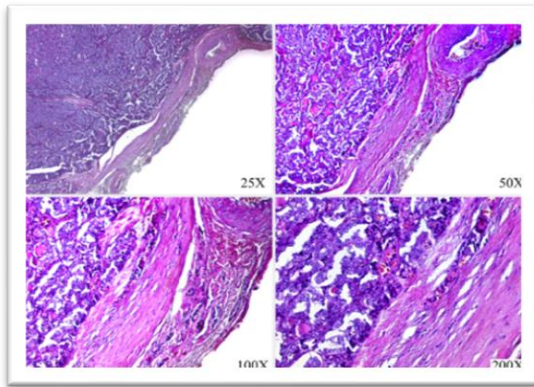
Fig. 4.5 Papillary thyroid carcinoma, follicular variant.– Hematoxylin & Eosin staining, magnification of: 25x, 50x, 100x and 200x
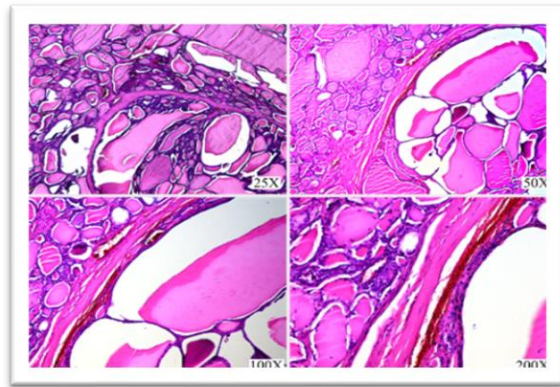
Fig. 4.6. Adenomatous nodule - Hematoxylin & Eosin staining, original magnification 25x, 50x, 100x and 200x

Difficult cases were also addressed, which required immunohistochemical tests to confirm the diagnosis (anisofollicular multinodular thyroid goiter with adenomatous nodule with oxyphilic cells - figure 4.14, papillary thyroid carcinoma, follicular variant, with oxyphilic cellularity - figure 4.19) and to make a differential diagnosis with other histopathological types of tumor proliferation or to detect collision tumors of medullary thyroid carcinoma associated with conventional thyroid papillary carcinoma - located in a single thyroid lobe (Figures 4.29 and 4.33)
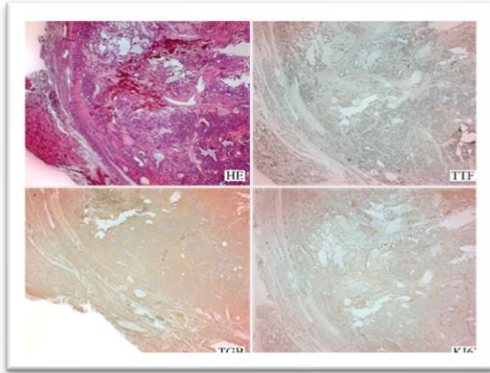
Fig. 4.14 Thyroid adenomatous nodule, fully encapsulated, adjacent parenchyma compressed by intraparenchymal encapsulated tumor proliferation - 10x original magnification (overview) - Hematoxylin & Eosin staining (top - left) and immunohistochemical tests with different specific markers (top - right) TGB (bottom - left), Ki67 (bottom - right).
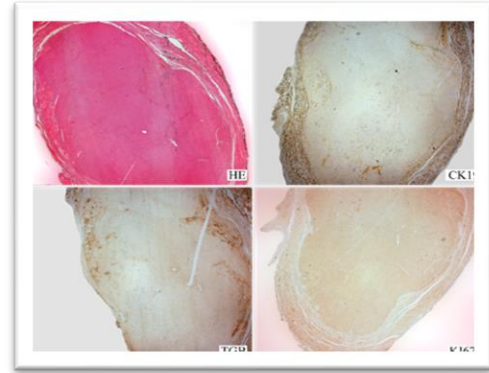
Fig. 4.19 Suspicious thyroid intraparenchymal nodule for papillary thyroid carcinoma - follicular variant, with oxyphilic cellularity - 10x original enlargement (overview) - Hematoxylin-Eosin staining (top - left) and immunohistochemical tests with different specific markers: top - right), TGB (bottom - left), Ki67 (bottom - right)
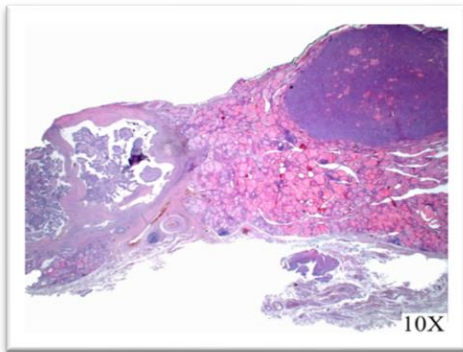
Fig. 4.29. Collision tumor - Hematoxylin-Eosin staining - original magnification 10x
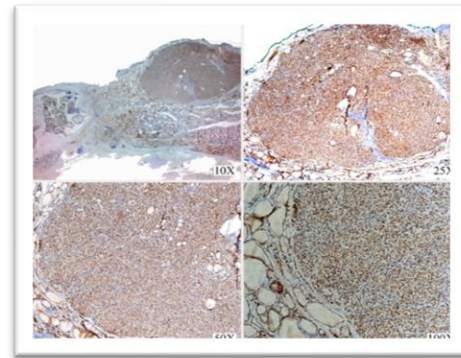
Fig. 4.33 Medullary thyroid carcinoma - original magnification 10x, 25x, 50x and 100x - Tumor cells and preserved follicular epithelium showed strong positivity for the immunohistochemical marker TTF1

4.2. Confocal Laser Scanning Microscopy (CLSM)

In this case, the images were acquired on marked (colored) samples and the fluorescence comes from Eosin. Thus, the signal from the sample has low specificity, coming from structures marked with Eosin (for example collagen, but also other structures - figures 4.59 and 4.58)
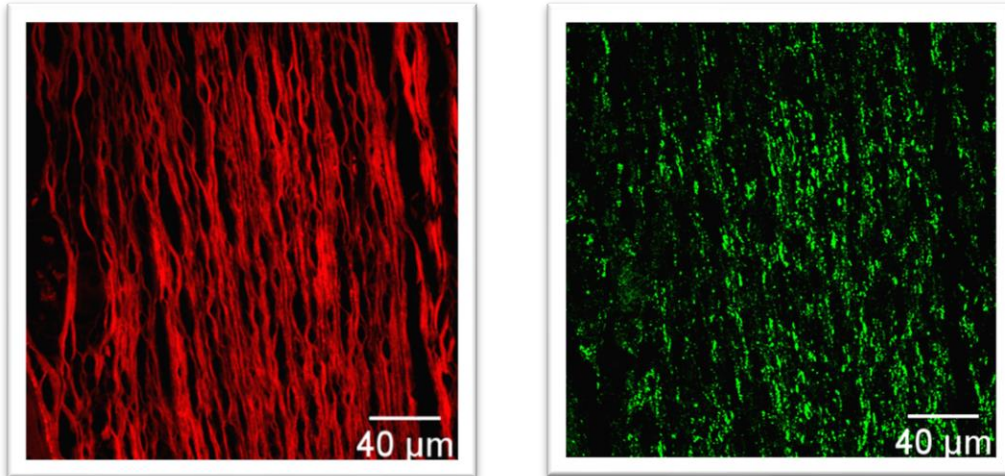
Fig. 4.59 Confocal microscopy images in fluorescence (left) and reflection (right) mode were acquired on the capsule of a malignant node (PTC). From the analysis of the reflection image, it is observed that it is difficult to interpret
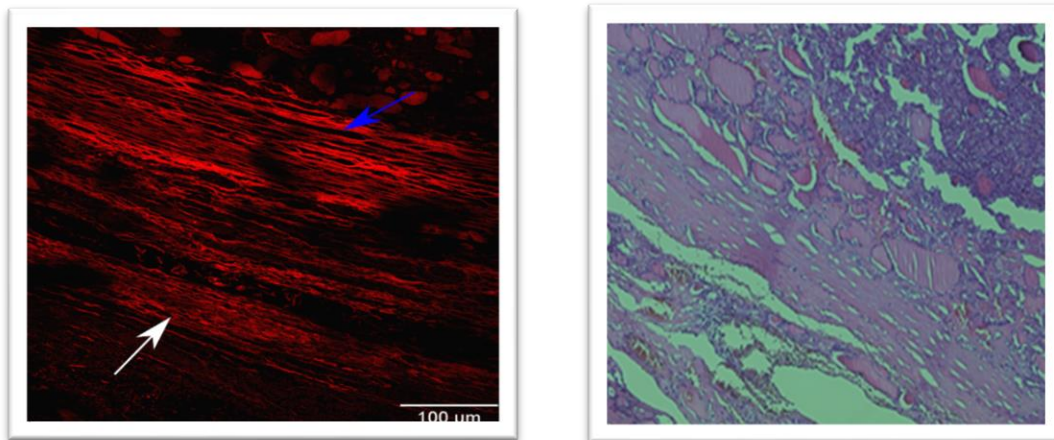
Fig. 4.58. Confocal microscopy image in fluorescence mode (left) in which both the thyroid gland capsule (white arrow) and the capsule of a malignant nodule (blue arrow) are visible, compared to the same region investigated using light microscopy (right).

We considered that this way of viewing the capsules is not specific and does not seem to be useful for investigations.

4.3. Two-Photon Excited Fluorescence (TPEF) Microscopy

In this case, too the samples are marked (colored), but the advantage of this method is that it can be obtained in parallel with the SHG and can show the distribution of collagen in the tissue, either marked and then we see Eosin or unmarked and then we see autofluorescent structures at the wavelength used, for example, collagen is autofluorescent in the ultraviolet. (figures 4.70 and 4.72).
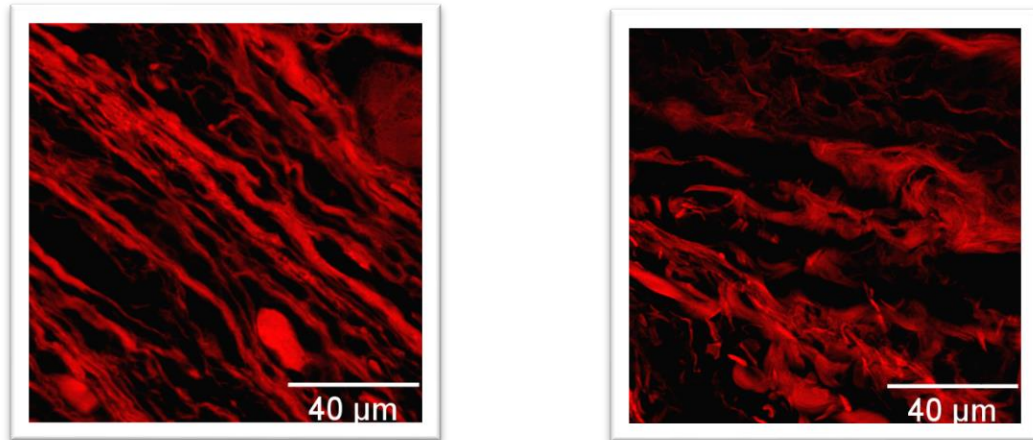
Fig. 4.70. TPEF images on the capsule of benign thyroid nodules.
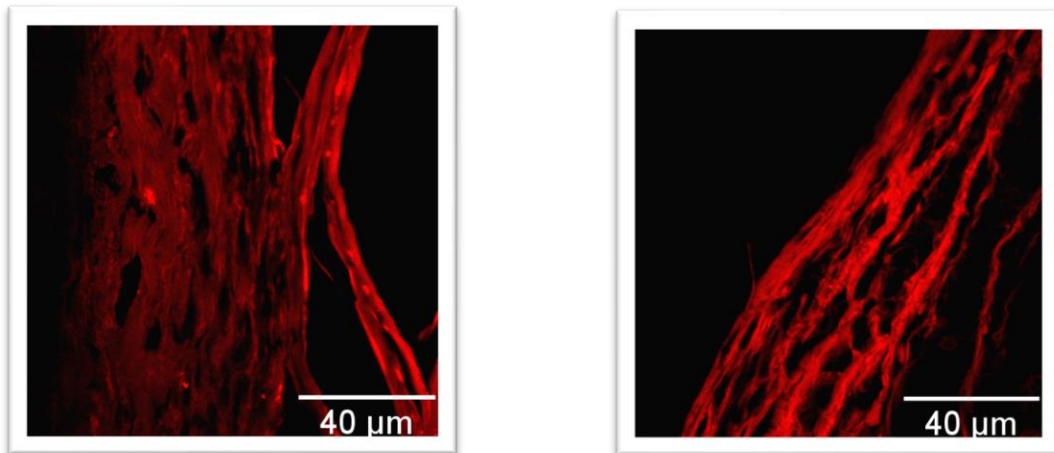
Fig. 4.72. TPEF images on the capsule of malignant thyroid nodules.

4.4. Second Harmonic Generation (SHG) Microscopy

We imagined and designed a procedure for extracting quantitative information regarding the orientation of collagen in thyroid tissue samples. The procedure was tested on capsules of malignant and benign thyroid nodules for their objective differentiation in five research studies.

In **STUDY NO.1** - we aimed the comparison between the capsule of malignant nodules (PTC) and benign (FA), using as METHOD: quantitative analysis of SHG images using fast Fourier transform (FFT).

Starting from an SHG image acquired on the capsule of a PTC node, respectively FA, we extracted the two-dimensional Fourier spectrum (2D FFT spectrum) and fitted it with an ellipse, where S is the small axis and L is the large axis) and we calculated an index collagen orientation, based on the ratio of the two axes (N = 1 - S / L), so the collagen orientation can be represented by an index ranging from 0 (random fibers) to 1 (perfectly aligned fibers).

We acquired images with second harmonic generation microscopy (Figures 4.77 and 4.78) that were used to evaluate the collagen orientation of tumor capsular thyroid nodules previously diagnosed as benign or malignant by conventional staining with Hematoxylin & Eosin.
.
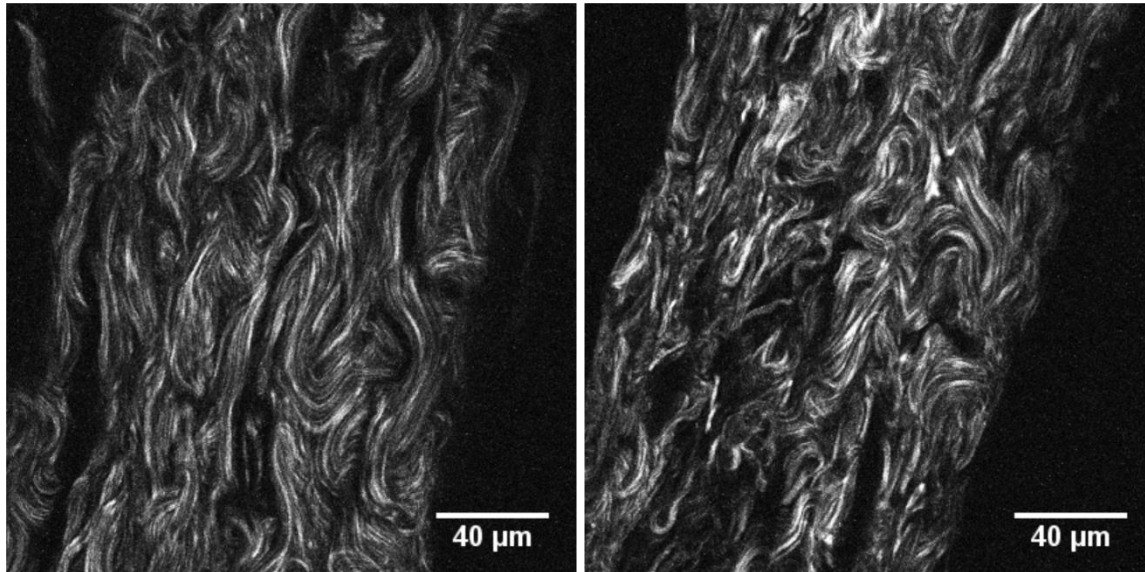
Fig. 4.77 Benign nodule capsule (images acquired by SHG microscopy)
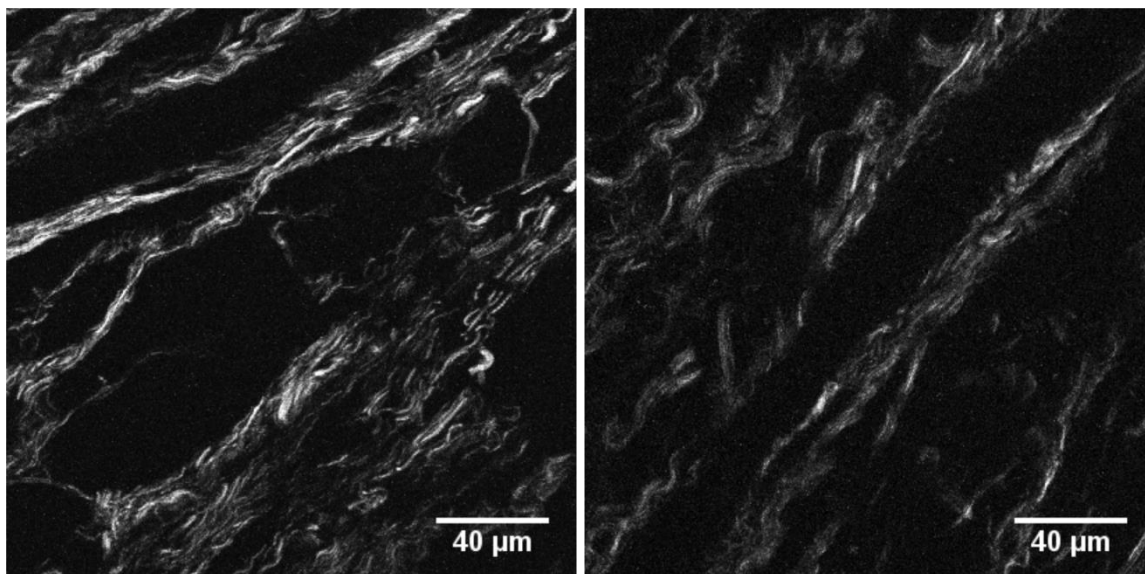
Fig. 4.78. Malignant nodule capsule (images acquired by SHG microscopy)

We calculated the FFT spectra for the images acquired by SHG microscopy for the considered pathologies (Figure 4.79).
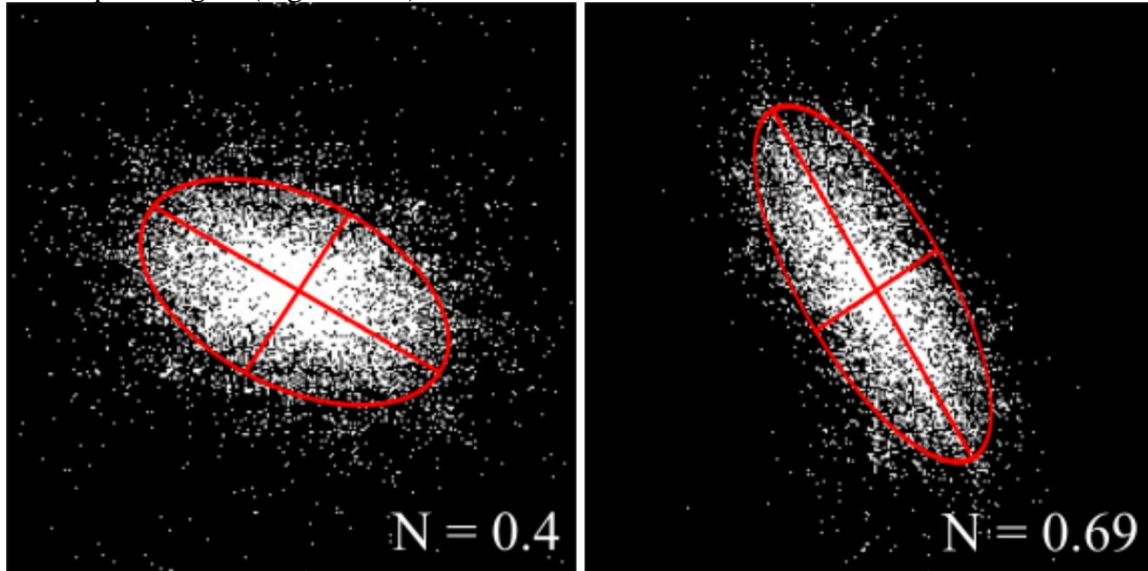
Fig. 4.79 The FFT power spectra images - benign nodule capsule (follicular adenoma) (left) and malignant nodule capsule (encapsulated papillary thyroid carcinoma) (right)

It can be seen in Figure 4.79 that the mean orientation of collagen (N) calculated from the FFT spectrum is higher for the papillary thyroid carcinoma capsule (N = 0.69) than for the follicular adenoma capsule (N = 0.4). FFT spectra were calculated for the entire image. We considered that, if the spectra are calculated for the lower regions of interest, a distribution of values can be obtained, depending on the degree of alignment for the collagen fibers in the regions of interest considered. On average, over a larger area, which is also the case for the entire analyzed area, it leads to a smaller N. Even if N was calculated on whole images, the results obtained show a difference in the organization of collagen between the two capsules.

In **STUDY NO.2** - we had the same PURPOSE: the differential diagnosis between the capsule of malignant nodules (PTC) and benign (FA), using as METHOD: an extended set of quantitative parameters (18) extracted from SHG images.

We compared the same capsular area (Figure 4.86) of the 2 types of microphotographs (with the optical microscope, respectively through the microscopy based on the generation of the second harmonic).
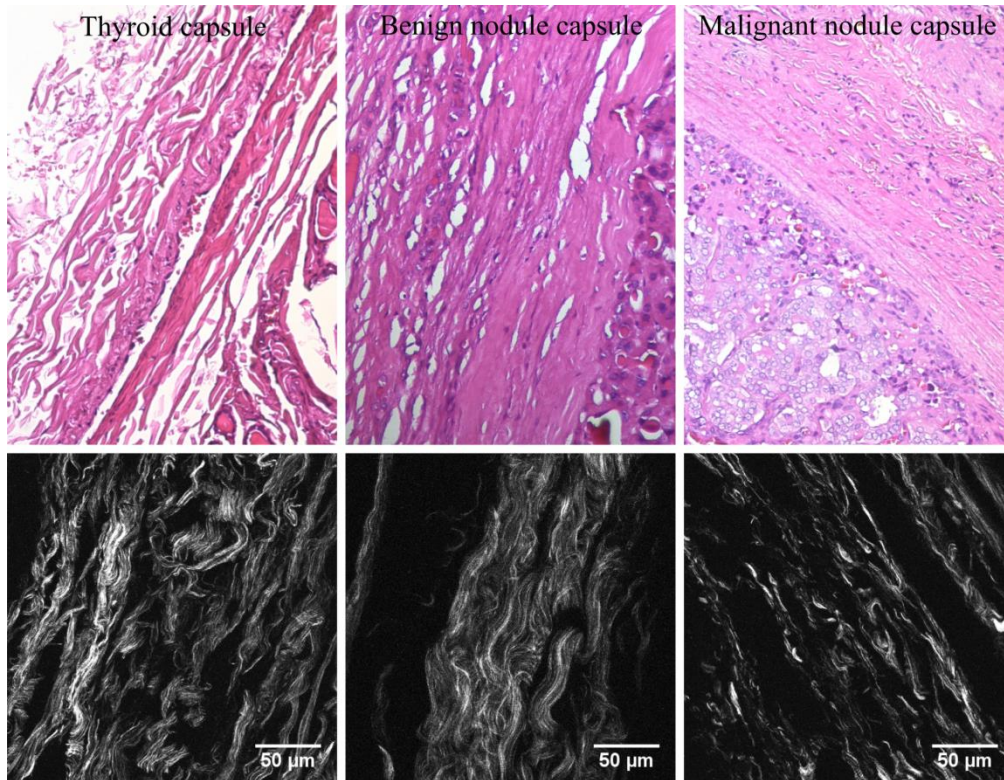
Fig. 4.86 Traditional H&E histopathology (upper row) acquired with a 20X objective and SHG microscopy images (lower row) for representative areas for the thyroid capsule, a thyroid follicular adenoma and a capsule surrounding a papillary thyroid carcinoma nodule.

A qualitative analysis of the investigated tissues and capsules showed a difference between the capsules of malignant and benign nodules, which is unidentifiable on images acquired with conventional light microscopy on sections stained with hematoxylin & eosin (Figure 4.86). Thus, we identified a wavy structure of collagen in the thyroid gland capsule that would allow deformation and normal growth of tissue, while providing resistance to deformation. A similar morphological structure can be observed in the capsules of benign nodules (follicular adenoma).
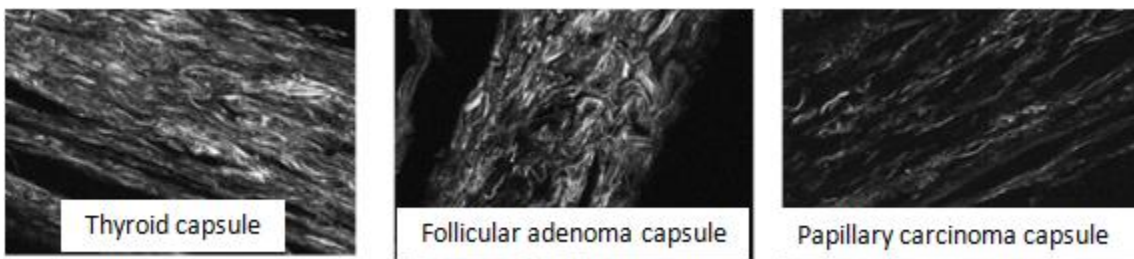
Fig. 4.87 Images acquired by SHG microscopy on the thyroid capsule (left), follicular adenoma capsule (middle) and papillary thyroid carcinoma capsule (right)

Comparative visual analysis in Figure 4.87 of images acquired by generating the second harmonic for the normal thyroid capsule and benign nodule reveals the wrapped collagen fibers, a collagen structure that is consistent with reports of collagen fibers in the breast tissue that allow

normal tissue deformation [8]. On the other hand, large, significant differences are observed in the distribution of collagen for the capsule surrounding a malignant node. In this case, in the image acquired by SHG microscopy, a very well directed and organized collagen structure is observed, with straight fibers.

This can be explained by the extensive expansion of collagen fibers due to the rapid growth of the malignant nodule or a reorganization of them as a defense mechanism against tumor expansion and infiltration, a reaction similar to that of peritumoral desmoplastic reaction.

Ultrastructural measurements were made at the level of capsular collagen fibers with several quantitative parameters on the images acquired by microscopy based on the generation of the second harmonic:

Table 4.1. Parameters used for the texture analysis of capsular collagen in SHG images.

		Parameter	Abbreviation
Histogram analysis		Mean	Mean
		Standard deviation	Hist-StDev
		Skewness	Hist-Skew
		Kurtosis	Hist-Kurt
Alternative collagen estimation		Ratio between the number of pixels with valaues above a threshold and the total number of pixels	TC-ratio
		Avearge value of SHG in significant areas	S-mean
Gray Level Co-occcurrence Matrix		Contrast	Contrast
		Inverse Difference Moment	IDM
		Angular Second Moment	ASM
		Entropy	Entropy
		Correlation	Correlation
Fractal analysis	on binary images	Fractal Dimension	FD-bin
		Lacunarity	Lac-bin
	on grayscale images	Fractal Dimension	FD-gray
		Lacunarity	Lac-gray
Helmholtz analysis		Standard deviation	Helm-StDev
		Skewness	Helm-Skew
		Kurtosis	Helm-Kurt

The distribution of collagen fibers in 2D images acquired by SHG microscopy was quantified by a set of parameters described above and listed in Table 4.1.

We tested their ability to characterize the organization of collagen in images acquired by microscopy based on the generation of the second harmonic and to differentiate benign encapsulated tumors from malignant ones.
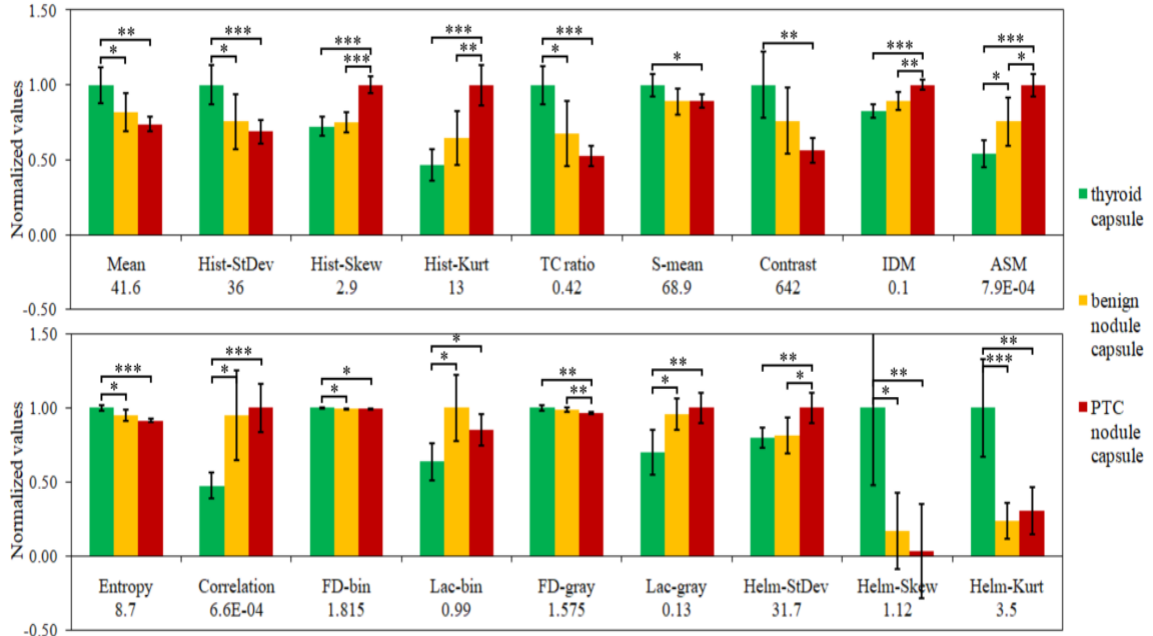
Fig. 4.88 Parameters computed from SHG image sets for the three investigated capsules. The vertical error bars represent the 95% confidence intervals. Under each parameter, the value with which they were normalized is shown. *p<0.05, **p<0.005, ***p<0.0005 are the p-values for the difference between two compared groups.

We tested the effectiveness of the quantification parameters described above in distinguishing between collagen from the thyroid gland capsule and capsules surrounding benign and malignant nodules, respectively (Figure 4.88).

Entropy is a measure of the disorder in the image (in this case). Let's note that this parameter did not indicate statistically relevant differences between malignant and benign on large images, but at the level of small images (full 512 x 512 pixel images were divided into 32 x 32 pixel areas) for the benign node obtains 3 distributions with average values at 6.44, ~ 7 and 7.45, and for the malignant node the component with high value (7.45) disappears, indicating a higher order, which, however, could not be highlighted at the level of the whole image, as shown in Figure 4.90.
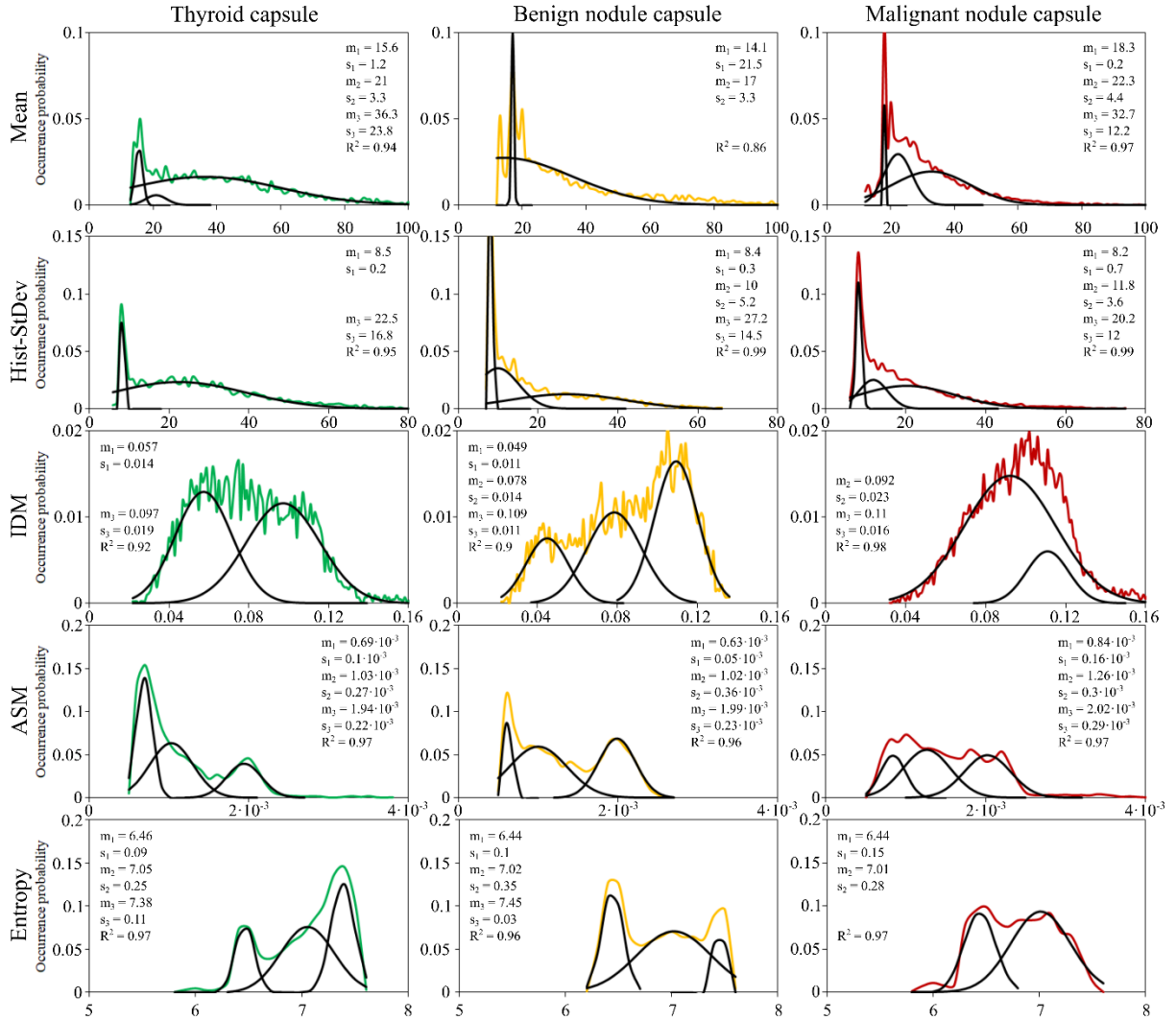
Fig.4.90 . Selected parameter distributions computed from the 32 x 32 pixels SHG image sets for the three investigated capsules. The black curves represent fitting Gaussians with their mean (m) and standard deviation (s) being given in the inset of each graph. A maximum of three Gaussians was fitted to each parameter distribution and the case with the maximum coefficient of determination (R2 is also given in the inset) is shown.

The results indicate a more "orderly" malignant capsule, with longer collagen fibers than the more wavy malignant capsule. Explanation: the organism's response.

The results we obtained, both qualitative and especially quantitative, indicate a morphology of collagen specific to the capsule surrounding the malignant nodules compared to the morphology of the fibrous capsule surrounding the benign nodules and possibly the thyroid capsule, more precisely indicates a capsule of the dense and thick thyroid gland, and pathological capsules with a smaller amount of collagen, with a capsule around the malignant nodule with more disparate collagen fibers.

In **STUDY NO.3** we had another aim, namely the early or participative identification of the invasion area in the PTC capsule, using the same METHOD as in RESEARCH STUDY NO. 2: an extended set of quantitative parameters (18) extracted from SHG images.

We compared the same capsular area of the 2 types of images (with the optical microscope, respectively with the SHG microscopy) (Figure 4.95):
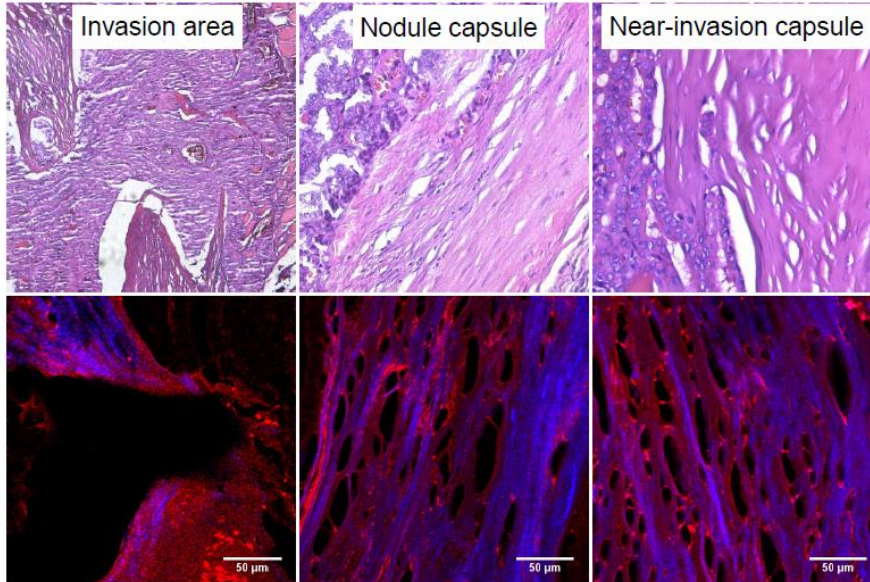
Fig. 4.95 Optical microscopy images (upper row) on tissue sections stained with Hematoxylin & Eosin and images acquired by SHG microscopy (lower row) for areas representative of the tumor-invaded capsular area of the malignant nodule, free capsular area, and the capsular area adjacent to the invasion area of the same studied nodule

We performed ultrastructural measurements at the level of capsular collagen fibers with the same quantitative parameters used previously (Table 4.1) on the images acquired by microscopy based on the generation of the second harmonic.

In this case, eight parameters calculated from images acquired by SHG microscopy provided statistically significant differences between the two investigated capsule areas (Figure 4.96), so we could discover a certain area to be invaded, in case of a possible transformation of a benign nodule.
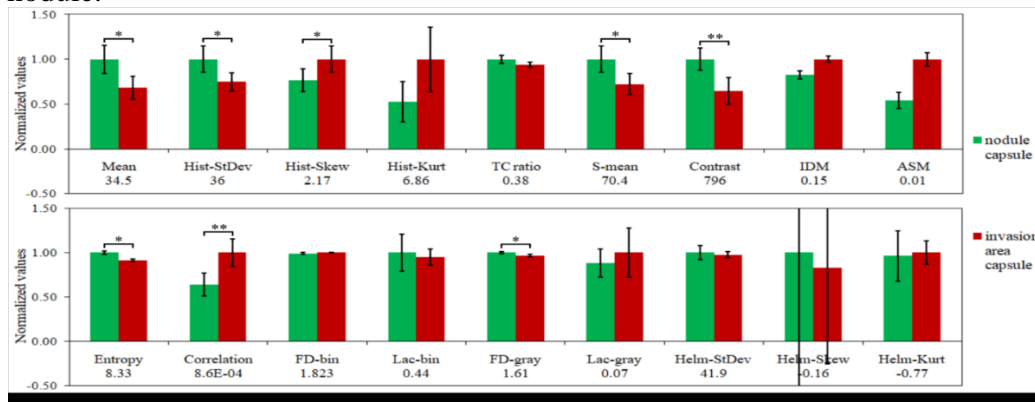
Fig 4.96 The parameters were calculated from the SHG images for the 2 regions of the investigated capsules. Vertical error bars represent 95% confidence intervals.

*Below each parameter has displayed the value with which they were normalized. * p <0.05, ** p <0.01, are the p values for the difference between two compared groups*

Conclusion: Quantitative methods of analysis of SHG images may provide clues to the areas of invasion before or without direct visualization of them in the tissue section under investigation.

In **STUDY NO.4** we had the same aim: the differential diagnosis between the capsule of malignant nodules (PTC) and benign (FA), but this time at a pixel level. The first three studies are related to full-image analysis (512 x 512 pixels) SHG with a first step made in study 2 of analysis on smaller images (32 x 32 pixels), but not at a pixel level.

We used as METHOD: polarization-dependent SHG microscopy (PSHG), followed by a fit of the experimental data with a theoretical model for collagen given in the formula:
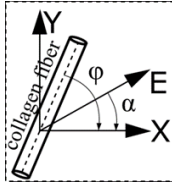
$$I = I_0 \left[\sin^2 2\,(\alpha - \phi) + \left(\frac{\chi_{31}}{\chi_{15}} \sin^2(\alpha - \phi) + \frac{\chi_{33}}{\chi_{15}} \cos^2(\alpha - \phi) \right)^2 \right]$$

which shows the dependence of the intensity of the second harmonic with the polarization angle (α), where φ is the angle made by the collagen fiber with the $0x$ axis, xy being the image plane, and E = the polarization direction of the laser radiation.

The method consists of having a set of SHG images and by fitting at a pixel level to obtain: the orientation of collagen fibers, ratios of elements of the tensor elements of order II susceptibility, and statistical analysis: mean, median value, scattering (StDev).

Attempts have been made to demonstrate that the imaging of collagen in thyroid nodule capsules at different angles of polarization of the laser beam with microscopy based on second harmonic generation describes a theoretical curve that can provide information about non-zero components of the second-order susceptibility tensor and fiber orientation of collagen. We used this approach in order to provide additional information about the collagen in the capsule of the studied thyroid nodules, which can complete the microscopy based on the generation of the second quantitative harmonic, based on the intensity and possibly the traditional histopathological examination.

A total of 10 areas were imagined: 3 for thyroid capsules, 3 for PTC capsules, and 4 for FA capsules. We collected images at different polarization angles of the laser beam between 0 and 180 degrees in 20-degree steps. An adapted Matlab custom code [13] was used to fit the experimental data in a pixel-by-pixel procedure with a theoretical curve.

The quality of the fitting procedure was quantified by the coefficient of determination R^2 (0 < R^2 <1), a value closer to the unit indicating a better fit. For each set of PSHG microscopy data, three new images were calculated only for those pixels with a good fit (R^2> 0.8): the collagen orientation angle (φ), one image for $\chi 31 / \chi 15$ and another for $\chi 33 / \chi 15$. χs are values in a tensor that characterize collagen in terms of generating the second harmonic. By tensor, we define a multidimensional matrix that characterizes the relationship between the intensity of SHG and the electric field of the excitation laser - the elements in the tensor. $\chi 31$, $\chi 33$, $\chi 15$ are the only non-zero values. χs result from processing a series of images recorded at different polarizations. By laser polarization, we define the direction of the oscillation of the electric field vector.

SHG images representative of the thyroid gland capsule, benign and malignant nodule are shown in Figure 4.97. Visual analysis of SHG microscopy images reveals wavy, disorganized collagen fibers wrapped around the thyroid capsule and benign nodule capsule, while a directional and organized collagen structure is identified for the malignant nodule capsule. These observations are not enough to differentiate the studied capsules. For the same test area, the differentiation

algorithm returned for each pixel three sets of results consisting of the fiber angle with respect to the linear polarization of the laser beam (φ) and two ratios of non-zero susceptibility tensor elements ($\chi31 / \chi15$, $\chi33 / \chi15$).
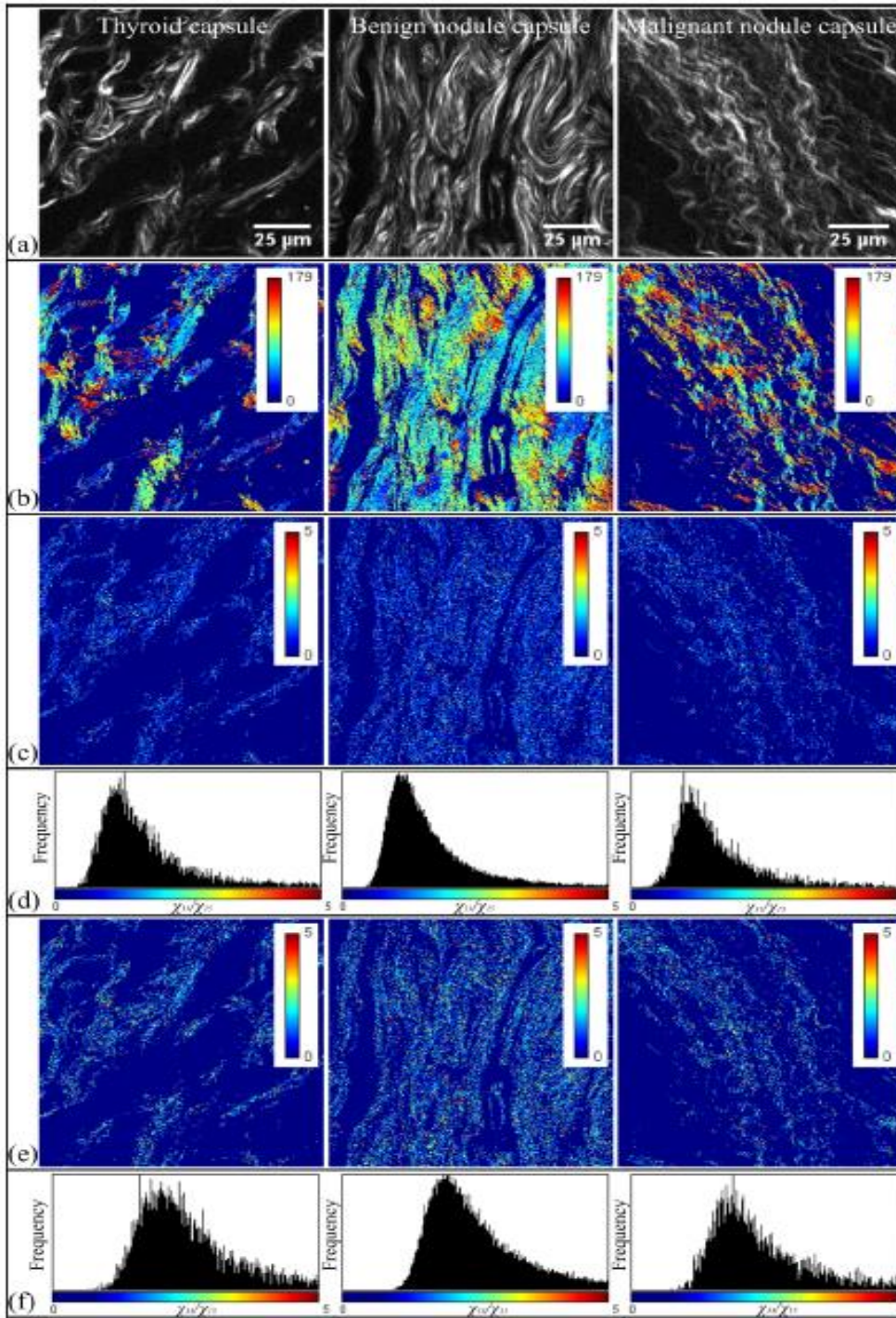
Fig. 4.97. PSHG microscopy images and resulting maps from the pixel-by-pixel fitting for the thyroid capsule, the benign nodule capsule, and the malignant nodule capsule. (a) SHG microscopy intensity image; (b) fibre angle map (φ); (c) $\chi31/\chi15$ maps; (d) $\chi31/\chi15$ map histograms; (e) $\chi33/\chi15$ maps; (f) $\chi33/\chi15$ map histograms.

The values χ_{31}/χ_{15} and χ_{33}/χ_{15} for each pixel in Figure 2.90 are displayed as color-coded maps in Figure 2.90 (c) and e), respectively. Figure 2.90 (d) and (f) show histograms (frequency of occurrence) for χ_{31}/χ_{15} and χ_{33}/χ_{15} which were calculated for pixels in all images obtained for the studied capsules. Because over 90% of the values with $R2 > 0.8$ are obtained for both χ_{31}/χ_{15} and χ_{33}/χ_{15}, between 1 and 5, the histograms shown are displayed only for this interval.

Tabel 4.3. Mode, mean and StDev values computed from the histograms of the two susceptibility tensor elements ratios. All the images acquired for the three capsules were considered when computing the histograms

	Parameter	Thyroid capsule	Benign nodule capsule	Malignant nodule capsule
χ_{31}/χ_{15}	Mode	1.303	1.042	0.989
	Mean	1.31	1.26	1.24
	StDev	0.47	0.44	0.44
χ_{33}/χ_{15}	Mode	2.035	1.903	1.856
	Mean	2.21	2.15	2.03
	StDev	0.67	0.6	0.6

Values: mode (most likely value in an image), mean, and standard deviation from a single Gaussian fit to histograms are given in Table 2.3. Mode values close to 1 are obtained for χ_{31}/χ_{15} in the case of nodular capsules, while a higher value is obtained for the thyroid capsule. Mean values are higher when matching histograms with a single Gaussian fit because the histograms are slightly inclined. No significant differences were observed in the standard deviations calculated for the three capsules. The mode values χ_{33}/χ_{15} for the thyroid capsule are significantly higher than the values for the nodule capsules, with a slightly higher value for the benign nodular capsule.

Changes in χ_{33}/χ_{15} values are observed between the capsules of malignant and benign nodules. Such changes have been interpreted as possible changes in the ultrastructure of collagen fibers. An increase of χ_{33}/χ_{15} was attributed to a redistribution of fibrils and collagen fibers in the laser focal volume [11]. Therefore, higher values of χ_{33}/χ_{15} and the standard deviation for the thyroid capsule may indicate a random organization of the capsular collagen of the benign thyroid and nodular gland and a malignant nodule capsule organized with aligned, parallel collagen fibers.

These results are consistent with those obtained for collagen fibers in nodular capsules when using SHG microscopy and texture analysis to determine the organization of collagen in the thyroid and nodular capsules [14]. The standard deviation obtained for χ_{33}/χ_{15} when comparing histograms with a single Gaussian match is higher for the thyroid capsule than for the nodular capsules, indicating a higher distribution of values, so once again greater disorganization in the distribution of collagen. The current results may seem in contradiction with those obtained in the previously cited literature [11], when the values for χ_{33}/χ_{15} indicated greater disorganization of collagen fibers in the case of malignant nodules. Those results were obtained from the distribution of collagen between the follicles (in the thyroid stroma) and inside the papillae in the case of thyroid papillary carcinoma, while the results obtained by us are on nodular and thyroid collagen capsules. Research shows that the current findings could be interpreted as an organization of collagen fibers in the capsules surrounding the malignant nodules as a defense of the body against

malignant tumors and that it indicates the same as in previous research studies a more wavy structure of collagen capsules in the benign case.

In **STUDY NO.5** - we had the same aim: the differential diagnosis between the capsule of malignant nodules (PTC) and benign (FA), also at the pixel level, only as in the same patient. METHODS: 1. polarization-dependent SHG microscopy followed by fitting with a theoretical model for collagen and 2. pixel-level collagen orientation analysis (to use images of the angular distribution of collagen fibers φ).

So far, studies have been performed on cases diagnosed in different patients, histopathological diagnoses, using light microscopy, AF or PTC. In this study, we selected the cases in which, on the same section of thyroid tissue, from the same patient, we identified by conventional light microscopy the malignant nodule among the other benign nodules (Figure 4.98). In this way we tried to eliminate the results of the recorded parameters supposed to be False-positive or False-negative, knowing that so far we have compared malignant nodules from one patient with benign nodules from another patient. Thus, we have results from the capsules of the two types of thyroid nodules (malignant and benign) in the sample from the same patient. We introduced in the study 3 cases (1 case = 1 patient) with both the malignant node and the benign node - detected on the same slide from the same patient, to exclude variability between patients. The images were digitalized with an automatic scanning system with a Leica APERIO LV1 light field microscope ("Aperio Whole Slide Scanner, Leica Biosystems") to determine the regions of interest that were further microphotographed under the PSHG microscope. For each patient, both malignant nodule and benign nodule capsules were studied and images were acquired for at least 7 regions of interest per node type per patient, resulting in a total of 25 regions of interest per node type. Each PSHG scan area was 125 x 125 µm2.
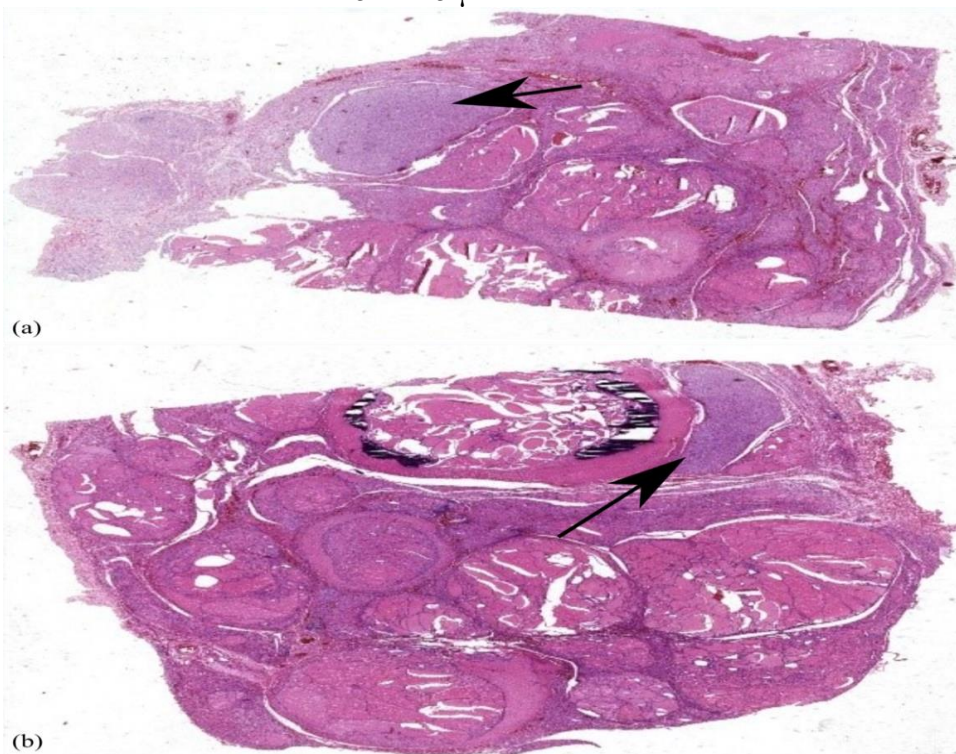
Figure 4.98 Blades with staining sections with Hematoxylin & Eosin, scanned with an automatic scanning system of Leica APERIO LV1 microscope slides.

In figure 4.98 we can see sections by polynodular, anisofollicular thyroid parenchyma with several adenomatous nodules, including a node (microfocus) encapsulated by papillary thyroid carcinoma (marked with a black arrow).

We took images on the same surface of the sample by laser scanning microscopy based on fluorescence generated by two-photon excitation (TPEF) and back-generated SHG, respectively with forward-generated SHG and superimposed the images to have a better view of the collagen distribution from the capsules of the benign nodules of the malignant nodules and the capsule of the thyroid gland.

We used the same method as in STUDY NO. 4 - namely the ratios of the elements of the susceptibility tensor to which we added another element of comparison, namely we tried to find a way to take into account the angle resulting from the algorithm used (we introduced a new parameter: Fi) (Figures 4.108 and 4.109). The main disadvantage of the calculation methods used so far from the orientation of collagen fibers is that they lack a reference for the angle of collagen in the case of the extracellular matrix, i.e. the orientation of the collagen fiber according to the orientation of the tissue. This angular information can only be used for particular situations, in the case of collagen fibers relative to the edges of the tumor, to provide diagnostic information [20]. Otherwise, the pixel-level information provided by such techniques is lost because the angular orientation is quantified only at the level of the entire image by using the distribution of angular values of collagen, such as standard deviation (e.g. to quantify skin aging [21]) or median absolute deviation (e.g., to differentiate between stages of small cell lung carcinoma) [22]).

From simple first-order statistics for pixel values, to statistics that take into account the spatial relationship of neighboring pixels (e.g., gray level correlation matrix (GLCM)) [6], [10] or even more advanced image analysis (e.g., fractal analysis [11], wavelet transform [12], Hough transform [13]) there are a multitude of methods for full-image quantification that have previously been used to analyze collagen distribution. On the other hand, using PSHG data sets one can calculate the anisotropic factor [9], [14], the degree of linear polarization [15] or the Stokes parameters [16] which are calculated at the pixel level, to estimate the alignment of molecular dipoles in relation to the polarization of the incident laser beam. Another approach referring to PSHG data sets requires theoretical models for collagen fibers [17], [18] and different fitting algorithms to determine the coefficients of the second-order nonlinear susceptibility tensor (χ (2)) for collagen with pixel resolution. Together with different coefficient ratios χ (2), this method calculates the orientation of the collagen fiber. Other less complex approaches also calculate the orientation of collagen fibers [19].

Recall that χ are values from a tensor that characterizes collagen in terms of generating the second harmonic (tensor means a multidimensional matrix that characterizes the relationship between the intensity of SHG and the electric field of the excitation laser - the elements in the tensor $\chi31$, $\chi33$, $\chi15$ are the only non-zero values). χ results from the processing of a series of images recorded at different polarizations (laser polarization is the direction of oscillation of the electric field vector).

Thus we introduced a new parameter: Fidefined as the angular distribution of collagen fibers in the acquired image. The color intensity shows angles 0-180 degrees (the more wavy the fiber in the image, the larger the color variations). (Figures 4.108 and 4.109)
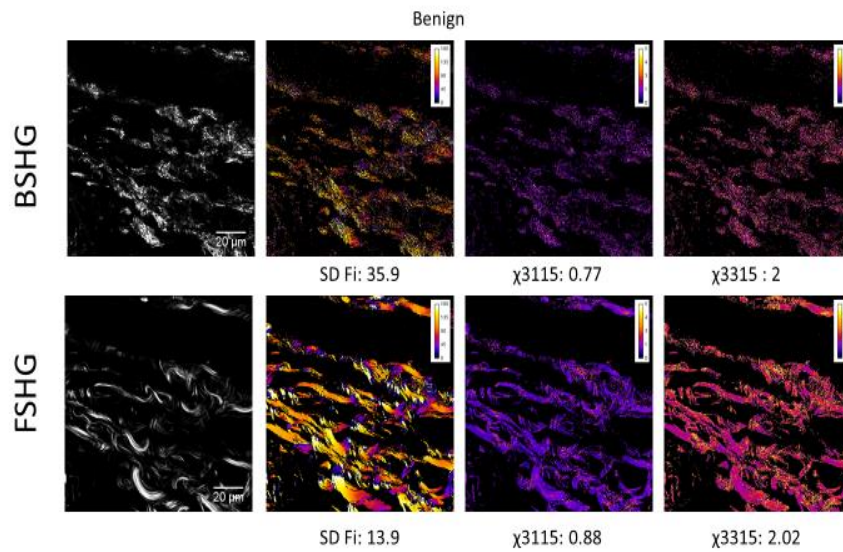
Fig. 4.108 Results obtained by the method of fitting the SHG intensity as a function of the polarization angle for the capsule of a benign node (FA - follicular adenoma); from left to right: 1) .images in SHG microscopy (upper left BSHG - SHG generated backwards, and lower left FSHG - SHG generated forward), 2). SD Fi - the angle of the collagen fibers, 3). χ3115 - Image obtained from the ratio of the susceptibility tensor elements χ31 and χ15, 4). χ3315 - Image obtained from the ratio of the χ33 and χ15 susceptibility tensor elements
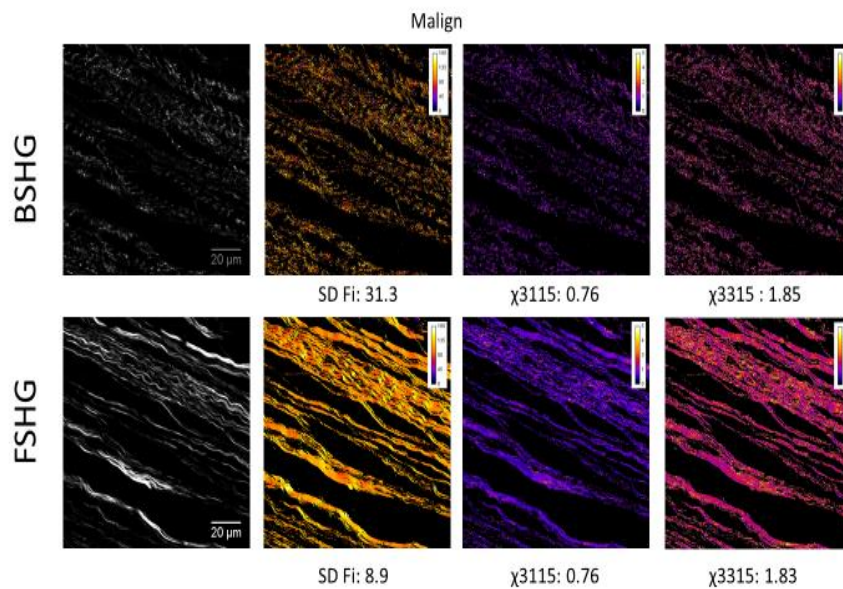
Fig. 4.109 Results obtained by the method of fitting the SHG intensity as a function of the polarization angle for the capsule of a malignant nodULE (PTC); from left to right: 1) .images in SHG (upper left BSHG - SHG generated backwards, and lower left FSHG - SHG generated forward), 2). SD Fi - the angle of the collagen fibers, 3). χ3115 - Image obtained from the ratio of the susceptibility tensor elements χ31 and χ15, 4). χ3315 - Image obtained from the ratio of the χ 33 and χ15 susceptibility tensor elements

Following the acquisition of PSHG image stacks, they were analyzed. A custom Matlab code [25] was used to fit the experimental data in a pixel-by-pixel procedure with a theoretical curve [26]. The model used for the SHG intensity dependence of collagen with the input polarization angle can be written as:

$$I_{SHG} \sim [\chi_{15} \cdot sin^2 2 (\alpha - \varphi) + (\chi_{31} \cdot sin^2 2 (\alpha - \varphi) + \chi_{33} \cdot cos^2 2 (\alpha - \varphi))^2]$$

where α is the angle of polarization incident of the laser beam, while φ is the orientation angle of the collagen fiber in the plane, and $\chi 15$, $\chi 31$, $\chi 33$ are the only non-zero components of the tensor nonlinear susceptibility (χ (2)) under the assumption of cylindrical symmetry of collagen.

Using this fitting procedure, we calculated pixel by pixel three images with the ratios of the susceptibility tensor elements ($\chi 31 / \chi 15$, $\chi 33 / \chi 15$ and $\chi 33 / \chi 31$), the image of the angular collagen distribution and the image of the coefficient of determination (R2).

To account for the distribution of collagen in a pixel-by-pixel approach, we used PSHG-acquired images to calculate a local dispersion of collagen fiber angles. Each pixel was replaced by the standard deviation (SD) or median absolute deviation (MAD) of the neighboring pixels in a square window with side l, where l takes odd values. We considered the following window dimensions: 3, 7, 15, 31 and 63. The resulting images were coded SD_l and MAD_l, if SD and MAD were used to account for local dispersion, respectively. While SD and MAD are both measures of statistical dispersion of a set of values, MAD is defined as the median of absolute deviations from the median and is less sensitive to extreme values than SD. If the dataset was normally distributed, SD is usually the best choice for evaluating the spread. However, if the data is not normally distributed, MAD is the most robust measure to use.

Several 14 different images were calculated for each stack of PSHG images for both forward and backward collection directions: three images χ (2), images φ, SD_l, and MAD_l images for five different l values. Another set of 14 images was obtained considering only pixels with R2> 0.8 after the fitting procedure.

The PSHG data sets were purchased in the regions of interest containing capsules of both malignant nodules (nodules of thyroid papillary carcinoma - PTC) and benign nodules (follicular adenoma - FA). Examples of images from collagen capsules surrounding both malignant and benign nodules are shown in Figure 2.103. The ratios of the susceptibility tensor elements were calculated for the PSHG data sets resulting in three new images on each region of interest (Figure 4.110).
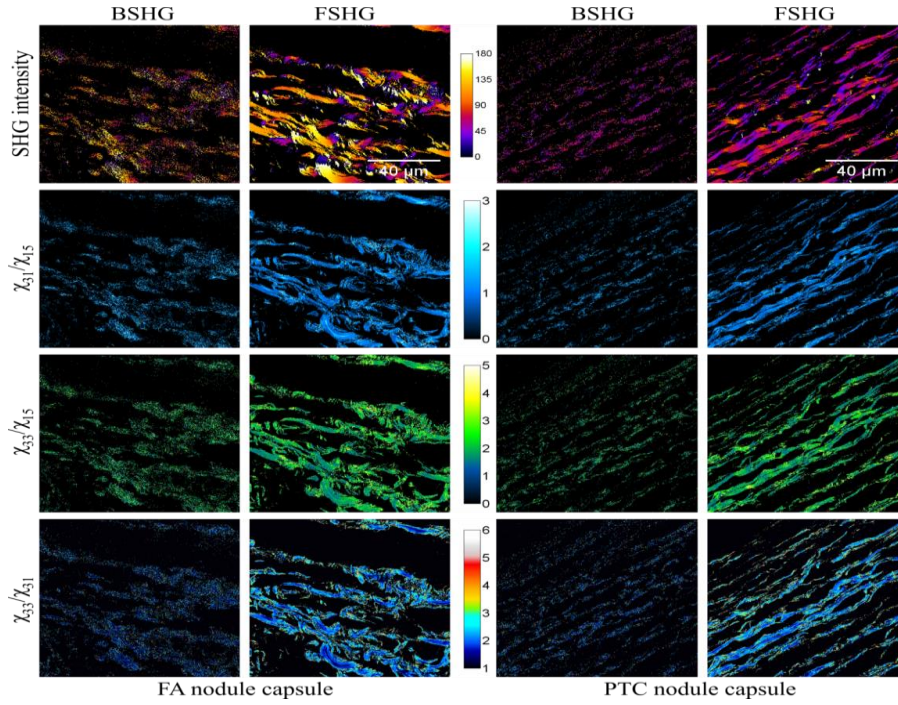
Fig. 4.110. Capsules surrounding FA and PTC nodules in PSHG microscopy. First row represents the SHG intensity images (averaging of all input polarization states) with the green and blue channels illustrating the BSHG and FSHG respectively, superimposed over the TPEF signal in the red channel. χ31/χ15, χ33/χ15 and χ33/χ31 are images obtained from the fitting algorithm with χ(2) element ratios computed for each pixel in the images.

We performed a pixel-level analysis on the images of the ratios of the susceptibility tensor elements χ (2). For the statistical analysis of the distribution of pixel values for the three types of images, we first tested the normality of the pixel samples. Because the normality test failed, which can be seen visually in Fig. 2.104, the whole distribution being positively inclined, we performed a non-parametric statistical analysis using the Mann-Whitney test. While for BSHG images, χ31 / χ15 did not return statistically relevant differences between PTC and FA nodular capsules, the other two reports for BSHG and all three for FSHG images showed statistically significant values in benign nodular capsules (follicular adenoma - FA), compared to malignant ones (papillary thyroid carcinoma - PTC). It has previously been shown that χ33 / χ31 is representative of the local anisotropy of the pixel sample [28]. At the same time, because the minimum value in the polarization dependence of the SHG intensity is Imin ~ (χ31 / χ15) 2, χ31 / χ15 can also be connected with the local anisotropy. An increase in both values can be explained by a decrease in local anisotropy in the case of benign nodular capsules (follicular adenoma - AF), compared to malignant ones (papillary thyroid carcinoma - PTC). This pixel-level result is consistent with previous results [6] where texture analysis on SHG intensity images revealed randomly arranged collagen fibers in benign nodule capsules and an organized capsule with collagen fibers aligned parallel to the malignant nodule capsule.

Although the ratio values of the elements χ (2) provided statistically relevant differences in five of the six situations considered, these parameters alone have almost no capacity to discriminate between malignant and benign nodule capsules, as the AUC is less than 0.6 (Fig. 4.111).
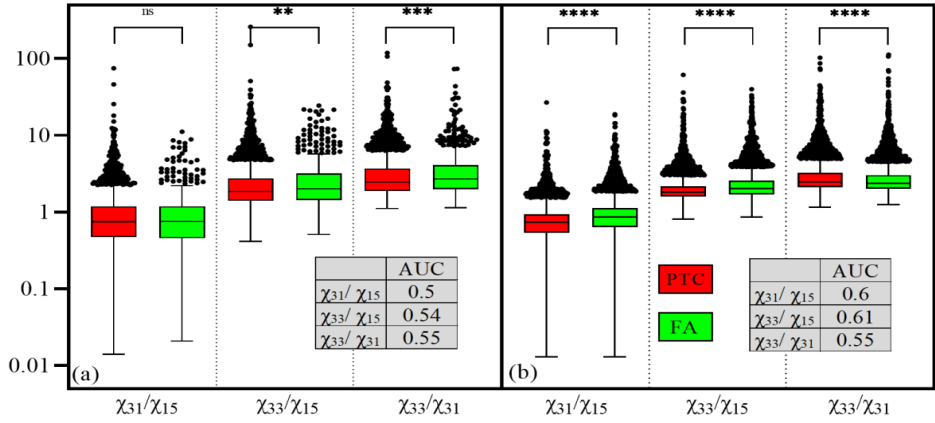
*Fig. 4.111. Statistical analysis of the χ(2) element ratios computed for each pixel from the PSHG datasets in the (a) BSHG configuration and (b) FSHG configuration. The insert in each graph provides the AUC values as a measure of the discrimination capacity of each ratio between PTC and FA nodule capsules. (ns p>0.05, ** p<0.01, *** p<0.001, **** p<0.0001).*

We also investigated the angular distribution of collagen in the capsules of the thyroid nodules selected for the study. The mean or median values of the orientation angle in the plane φ depend on the orientation of the sample and thus cannot provide useful information. On the other hand, measures of the distribution of the orientation angle, such as standard deviation (SD) and median absolute deviation (MAD) were extracted from whole images to quantify the morphology of the collagen fibers in the sample.

As can be seen in Fig.4.112, both SD and MAD values for capsules surrounding malignant nodules (PTC) are lower than for capsules of benign nodules (FA), indicating that collagen fibers are less wavy in malignant nodules capsules. This is also visible from the SHG intensity images in Figs. 2.103 and is in line with the results presented above [6]. Although the difference between capsules surrounding malignant (PTC) and benign (FA) nodules is not statistically significant for SD in BSHG images, there are statistically significant differences between the collagen fiber distributions of capsules surrounding malignant (PTC) and benign (FA) nodules quantified by MAD. One possible explanation would be that MAD is less sensitive to extreme values than SD, confirmed by lower MAD values. A possible source of such values in φ images may come from the fact that the range in which the pixels have values is (0, 180 °), more precisely from the adjacent pixels where the transition from 0 to 180 ° took place.
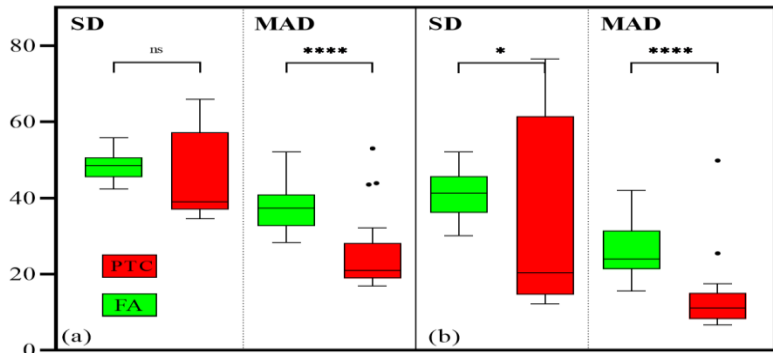
*Fig. 4.112. Angular distribution of collagen estimated on whole PSHG datasets from φ images using different metrics: standard deviation (SD) and median absolute deviation (MAD) in the (a) BSHG configuration and (b) FSHG configuration (ns p>0.05, * p<0.05, **** p<0.0001).*

Because the PSHG data fit algorithm calculates the collagen orientation in each pixel, information is lost only by considering measures of the orientation distribution in entire images. With this in mind, we calculated local pixel-by-pixel collagen orientation distributions using both SD and MAD to quantify fiber distribution. Considering this procedure, images were obtained with the local orientation of the collagen (fig. 4.113) depending on the calculation window for distribution (images SD_l and MAD¬¬_l, where l is the size of the window).
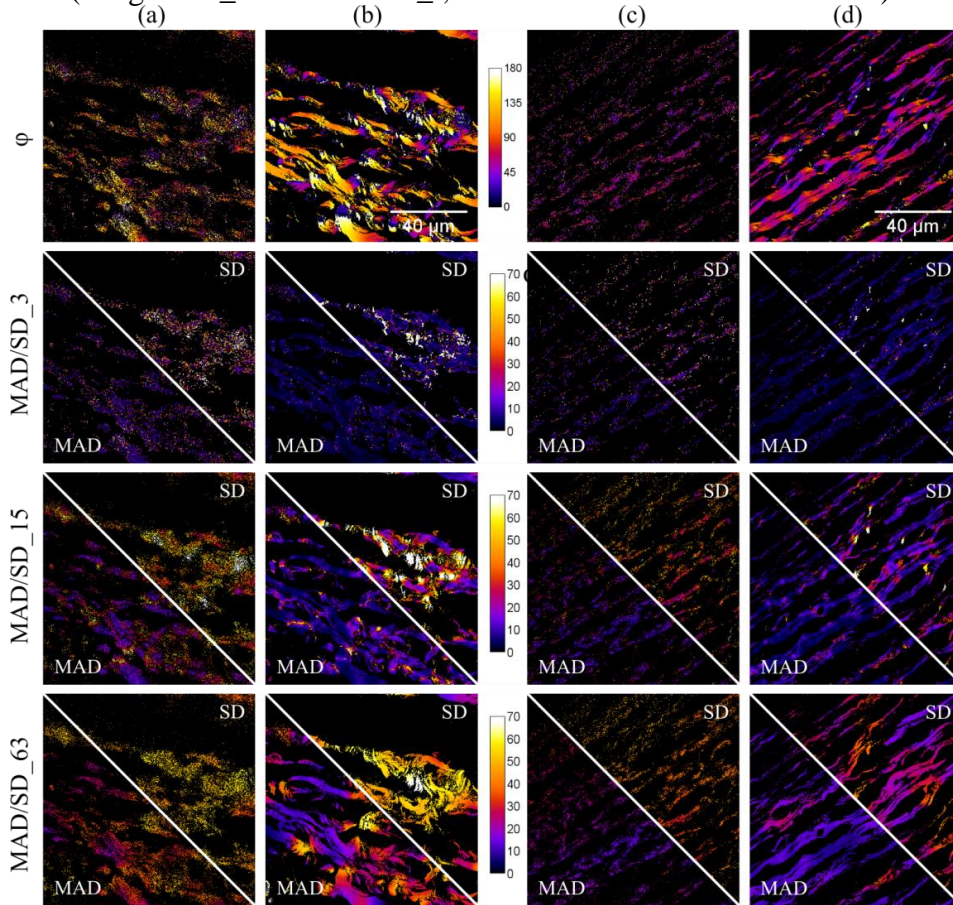
Fig. 4.113. Collagen orientation distribution imaging in PSHG datasets. The same regions of interest as in Figure 2.103. are considered for both malignant nodular capsules (PTC) and benign ones (FA). The first row represents the angular distribution of collagen (φ), calculated from the fitting algorithm. SD_l and MAD_l images with SD / MAD computation window sizes l = 3, 15 and 63 pixels are shown for comparison

The Pearson linear correlation test showed a moderate correlation between SD and MAD values for the BSHG case (0.62 for a 3 x 3 pixel SD / MAD calculation window) and a weaker correlation for FSHG (0.4 for the calculation 3 x 3). For both SHG collection configurations, the correlation between SD and MAD increases with the calculation window. For example, for the 63 x 63 pixel window, the two parameters were strongly correlated for benign nodule capsules (0.9 for BSHG and 0.8 for FSHG) and moderately correlated for nodule malignant capsules (0.7 for BSHG and 0.62 for FSHG). Enlarging the calculation window for both SD and MAD, leads to an increased number of pixels considered from a maximum of 9 pixels in the 3 x 3 window to almost 4000 for the 63 x 63 window. a larger sample to be closer to a normal distribution (fewer values); hence a stronger correlation between SD and MAD with increased window size. A stronger correlation between SD and MAD for the benign capsule than for the malignant capsule suggests

that the orientation distribution is closer to a normal distribution. These results are determined by the undulation of the collagen distribution, with a higher degree of disorganization for the benign nodular capsule. The previous assumption of normality for orientation distributions is confirmed by calculating a simple linear regression between the SD and MAD data sets. We obtained a slope of 1.403, close to the theoretical value of b = 1.4826 for a normal distribution.

We performed statistical analyzes at the pixel level with pixel samples from SD / MAD images. For the statistical analysis of the pixel value distribution for the five image types for each SHG collection configuration, we first tested the normality of the pixel samples. Because they failed the normality test, which can be seen visually in Fig. 2.107, the whole distribution being positively inclined, we performed non-parametric statistical analyzes using the Mann-Whitney test.

For FSHG images, all images obtained for different sizes of the SD / MAD calculation window indicate more statistically relevant values for benign nodule (FA) capsules compared to malignant nodule (PTC) capsules. The results are similar for BSHG images, except for the smallest calculation window we considered (l = 3). These pixel-level results confirm previous results on whole images and indicate that the local distribution of collagen is the same as the distribution of the whole image, with a different collagen curl between the malignant (PTC) and benign (FA) nodular capsules.
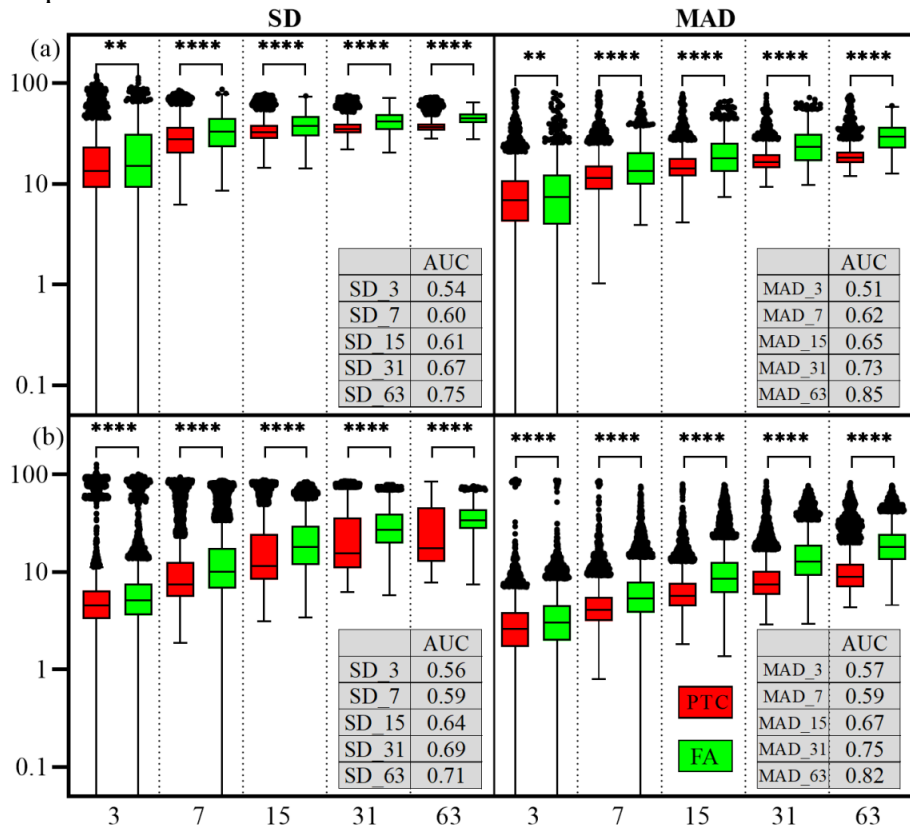
Fig. 4.114 Statistical parameters extracted from the pixel-level orientation analysis of collagen in PTC and FA nodule capsules. Both SD_l and MAD_l images are considered with computation window size l = 3, 7, 15, 31 and 63 pixels are shown for comparison in (a) BSHG and (b) FSHG datasets. (** p<0.01, **** p<0.0001)

All the SD / MAD pixel datasets provided statistically relevant differences between the PTC and FA nodule capsules. Despite these, for low SD/MAD computational windows (l = 3, 7) there is almost no discrimination capacity between malignant vs. benign capsules since the AUC is less

than 0.6 (inserts in Fig. 2.107). As the window size increases the discrimination capacity increases as well with the highest values obtained for MAD and FSHG images. For almost all considered situations (except for l = 3 in BSHG images) MAD proves better discrimination capacity between PTC and FA than SD.

The texture analysis was performed on the image φ, the three images of the ratio of the elements of the susceptibility tensor χ (2), the five MAD images, and five SD for both BSHG and FSHG configurations. At the same time, we calculated images that retain only pixels corresponding to R2> 0.8, exactly as obtained from the fitting algorithm. SHG intensity images were not considered, because the analysis of the texture of full intensity SHG images was presented in STUDY NO. 2, described above [6].

Chapter 2 – Conclusions

The investigations presented in this thesis focused on the study of biological samples with thyroid pathological tissue using microscopic techniques with laser beam scanning. This research topic addresses a sensitive topic of thyroid pathology, namely the development of a histopathological diagnosis as accurate as possible of encapsulated thyroid nodules, it is known that the pathologist often suffers from a lack of total visualization under the light microscope of the thyroid capsule that delimits the tumor nodule from the adjacent thyroid normal parenchyma.

The importance of the results obtained is due to the interdisciplinary collaboration and the consistent application of a working standard in all the experiments in this paper. Quantitative parameters of the images acquired on the capsule of the thyroid nodules and thyroid gland were used, which allowed the analysis of collagen in their composition, obtaining statistically significant results in comparing the structural change and its distribution.

These results suggest, for the first time in the literature, that some thyroid tumor nodules can be differentiated only by studying their capsule, without the need for tumor cell morphology, an indispensable element in developing the histopathological diagnosis of certain tumor lesions.

5.1 - Results

We have approached several optical microscopy techniques such as confocal microscopy, laser scanning microscopy based on two-photon excitation fluorescence (TPEF), second scanning laser scanning microscopy (SHG), and laser-based scanning microscopy on the generation of the second harmonic dependent on the excitation laser radiation polarization (PSHG) to observe possible unidentifiable capsular changes with traditional classical light microscopy, in order to differentiate the benign and malignant encapsulated tumor nodules.

In classical light microscopy, photomicrographs were obtained from the cases selected for research, as well as for difficult cases, for which IHC tests were required for a final histopathological diagnosis, elaborating in each case the histopathological diagnosis following the microscopic examination, followed by the elaboration of a complete histopathological diagnosis on the standard Hematoxylin & Eosin staining correlated with the IHC tests.

In CLSM the images could be interpreted, in the sense that we could detect the capsule surrounding the tumor nodule, the thyroid gland capsule, and structures compatible with those of the thyroid follicles inside the tumor nodule, but also from the adjacent thyroid parenchyma, but without

being able to make a differential diagnosis between their normal, benign or malignant character, not providing additional information compared to conventional fluorescence microscopy.

In confocal reflection microscopy, the images were difficult to interpret because we had no contrast in the image.

TPEF microscopy brought overview images of thyroid tissue, because fluorescence has the advantage that it can give an overall image, showing other tissue structures besides collagen highlighted by SHG microscopy. The TPEF images and SHG images were studied separately, but also superimposed to cumulate the information provided on the one hand fluorescence, and on the other hand, according to the nonlinear nature of SHG, by obtaining a three-dimensional resolution (3D images);

In **study no. 1** we used the fast Fourier transform (FFT) analysis of the acquired images by generating the second harmonic for the capsule of the thyroid papillary carcinoma nodule and the benign nodule. And in this case, we found statistically significant results. The average orientation of collagen (N) calculated from the FFT spectrum is higher for the follicular adenoma capsule (N = 0.69) than for the thyroid papillary carcinoma capsule (N = 0.4). FFT power spectra were calculated for the entire image. We considered that if the spectra are calculated for the lower regions of interest, a distribution of values can be obtained, depending on the degree of alignment for the collagen fibers in the regions of interest considered. On average, over a larger area, which is also the case for the entire analyzed area, it leads to a smaller N. Even if N was calculated on whole images, the results obtained show a difference in the organization of collagen between the two capsular types.

SHG microscopy is the most efficient method, because, in addition to the better imaging signal than in the case of fluorescence imaging, it is very sensitive to structural information of the examined sample, in our case collagen on to which we can analyze quantitative changes using different parameters from 4 methods of textural analysis of an image (image histogram, "Gray Level Correlation Matrix" (GLCM) analysis, fractal analysis and Helmholtz analysis), used starting with **study no. 2**.

The pixel intensities of the parameter "Average SHG" - (average), were lower, obtained for both FA and PTC capsules, with statistically significant differences in terms of thyroid capsule. These are an indication of a lower SHG signal in the two pathological conditions studied, either due to a decrease in collagen density, or a decrease in the SHG signal on individual collagen fibers, or both. Calculating two other parameters, namely "TC-ratio" (the ratio between the number of pixels with values above a threshold and the total number of pixels) and "S-mean" (average value of SHG in significant areas) we tried to answer this question. The "TC-ratio" estimates the total area of collagen in an SHG image and only accounts for changes in collagen density. For this parameter, a statistically significant decrease was obtained between the thyroid capsule and both pathological nodular capsules. This result is consistent with the thinner capsule in the case of the benign nodule and the lower density of collagen fibers for the PTC capsule, without being able to distinguish between them. On the other hand, "S-mean", which would show changes in pixel intensity only on areas covered by collagen, indicates a statistically significant decrease in the SHG signal when comparing the thyroid capsule with the PTC nodule capsule. The lower value of "S-mean" may occur due to the reorganization of collagen fibers, either by loss of crystallinity or by a greater disturbance in the focal volume.

The "Hist-StDev" parameter (standard deviation) was used to quantify the amount of dispersion of the data set. Usually, a smaller standard deviation of a pixel intensity distribution is a sign of a clearer image, which in our case could indicate a more widespread distribution of individual

collagen fibers. This is the situation of the PTC nodule capsule which has a standard deviation - "Hist-StDev" statistically significantly lower than the thyroid capsule.

Regarding the "Hist-Skew" parameter (asymmetry index), all three distributions are strongly positive. A higher value for this parameter shows a darker image [34], therefore, the intensity of the SHG signal on collagen is lower or a lower density of collagen in the imaging area. The higher value of the "Hist-Skew" parameter for the PTC capsule is consistent with the observation of thinner and more dispersed collagen fibers inside the PTC capsule.

All three distributions studied had the parameter "Hist-Kurt" (flattening index), high positive. We observed a statistically significant increase from both the thyroid capsule and the FA nodule capsule to the PTC nodule capsule indicating that the pixel distribution is closer to average than for a normal distribution, and a small part of the variation is caused by extremely rare deviations.

A lower level of the "Hist-StDev" parameter (standard deviation), correlated with a higher level of the "Hist-Kurt" parameter (flattening index), indicates a narrower distribution of pixel values around the mean and as for "Hist-StDev", it indicates clearer features regarding the distribution of collagen fiber in the image.

The advantage of using the parameters of the shape of the distribution, such as the parameters "Hist-Skew" (asymmetry index), and "Hist-Kurt" (flattening index), is that they are independent of intensity and thus more robust in characterizing the structural patterns of capsular collagen.

While first-order statistical parameters calculated using the image histogram are directly related to the distribution of the gray level in the image, second-order statistical parameters depend on spatial arrangements and the correlation of intensities between pixels.

The contrast parameter ("Contr") is associated with the average gray difference between the neighboring pixels and quantifies the heterogeneous distribution of collagen present in the image. A higher contrast ("Contr") indicates highly contrasted images, which can be associated with features that are distributed without a preferential alignment [25]. A statistically significantly higher contrast ("Contr") was obtained for the thyroid capsule than for the PTC capsule, which can be explained by the presence of aligned collagen fibers in the PTC capsule.

The parameter "IDM" - "Inverse Difference Moment" quantifies the local similarities in the SHG image and in our experiment, although "Contr" and "IDM" are inversely correlated, "IDM" is able to provide differences statistically significant between benign and malignant nodule capsules, while "Contr" is not capable.

The parameter "ASM" - "Angular Second Moment" (energy or second angular momentum) detects disturbances in textures, reaching a maximum value equal to that which occurs when the distribution of the gray level is homogeneous. The lower values of "ASM" are due to a higher number of small entries in the "Gray Level Co-occurrence Matrix" (GLCM) and are an indication of heterogeneous images, in our case distributions less homogeneous collagen. "ASM" is the only parameter that reflects a statistically significant increase from the corresponding value

A larger entropy ("Ent") indicates a more complex image texture, as in the case of the contrast "Contr" and "IDM", although "ASM" and the entropy ("Ent") are inversely correlated, "ASM" is able to provide statistically significant differences between the three classes considered, while entropy ("Ent") is not.

The correlation statistical parameter ("Corr") is a measure of the linear dependencies of the gray levels in the image. All three studied capsules returned low correlation values. Because a low correlation ("Corr") generally means independent adjacent gray levels, no significant regular pattern can be identified in the image.

To use the ability of the correlation parameter ("Corr") to detect common patterns in an image, we compared the correlation values ("Corr") of the "Gray Level Correlation Matrix" (GLCM) occurrence Matrix at different pixel distances, and we matched the correlation-distance dependence (its dependence with the distance between pixels) with an exponential curve to calculate its decrease rate. Quantitatively, the correlation ("Corr") for the PTC capsule decreased with a steeper slope suggesting distinct linear fibers, while for the FA capsule the correlation remained high as the pixel distance increased, suggesting a more disorganized fibrous collagen structure.

The fractal analysis was computed both on grayscale images ("FD-gray" and "Lac-gray" parameters) and on binary images ("FD-bin" and "Lac-bin" parameters) obtained from the picture. Although binary analysis is the most used, one of its disadvantages (for example, the need for a threshold for image binarization) has also been encountered in our case. None of the "FD-bin" and "Lac-bin" parameters could detect significant differences between malignant and benign nodule capsules. One possible explanation is that for the binary image, the "FD-bin" parameter provided information about the texture of the edges in the binary image, rather than the texture of the collagen distribution, which is the case in a previous study that addressed tumor cell membrane investigations. On the other hand, we considered that gray images are more suitable for fractal analysis when determining the texture of collagen distribution. The "FD-gray" parameter showed a significant decrease in the complexity of the PTC nodule capsule compared to both the thyroid gland and the FA nodule capsule. The "Lac-gray" parameter increases for the capsule of tumor nodules, with a higher value for malignant nodules, a result that is consistent with those obtained for the parameters "TC-ratio" and "S-mean" discussed above.

Statistically significant values were also recorded for the parameters used in the Helmholtz analysis. In the case of the thyroid gland capsule, the parameter "Helm-StDev" (standard deviation) is higher, associated with the parameter "Helm-Skew" (asymmetry index) moderately increased ("Helm-Skew" = 1.12), and for nodular capsules the distributions approximately symmetrical ("Helm-Skew" < 0.5) and "Helm-Kurt" significantly lower, indicate a higher value of dispersion in the collagen distribution with a significantly higher value for the PTC capsule. This result is consistent with a possible reorganization of collagen fibers, either by loss of crystallinity or by a larger focal volume disturbance that could be indicated by "S-mean".

Not all quantification parameters could differentiate between FA and PTC capsules. One possible explanation is that the structural changes in collagen could be dispersed in large-scale imaging, so we tested the parameters on small-scale SHG imaging for the benign and malignant nodule capsules and the explanation proved to be valid.

Although, when calculated for the entire SHG image, the "MedieSHG" parameter (decreased) for the PTC node capsule, for small-scale images, there is an obvious shift in the average distribution to higher values. This result can be attributed to a small-scale change in the organization of collagen in the focal volume, contrary to the conclusion drawn from the "MedieSHG" calculated on the entire image.

A common component, the parameter "IDM" - "Inverse Difference Moment" (homogeneity or moment of inverse difference) around 0.11 was obtained for both benign and malignant distributions. On the other hand, higher "IDM" values-centered at 0.092 are obtained for the PTC nodule capsule, with two regions centered at 0.049 and 0.078 resulting in benign nodules. These results confirm the statistically significant increase of the "IDM" parameter, for the PTC nodules obtained on whole SHG images. Similar results are obtained for the parameter "ASM" - "Angular Second Moment" (energy or second angular momentum) with a high-value component ($\sim 2 \cdot 10^{-3}$) present for both FA and PTC

capsules, while the other values are distributed between $0.63 \cdot 10\text{-}3$ and $1.02 \cdot 10\text{-}3$ for the FA capsule and $0.84 \cdot 10\text{-}3$ and $1.26 \cdot 10\text{-}3$ for the PTC capsule, respectively. The small-scale analysis of the "ASM" and "IDM" parameters indicates a feature for PTC nodules: local areas with a higher "IDM" attributed to a high similarity and areas with a higher ASM, allocated to more homogeneous regions. Thus, we assume that the distribution of collagen undergoes significant changes on a small scale, which could be missed by quantifying large field images.

In the case of the "Ent" parameter (entropy), although the values obtained on the whole SHG image were not statistically different for the benign and malignant capsules, when we calculated this parameter on smaller images, we obtained a significant difference between these two capsules. While the distributions centered at 6.44 and ~ 7 are present in both cases, a higher "Ent" (entropy) (~ 7.45) is obtained only for the capsule of the FA node that indicates more complex small-scale image textures, consistent with the corrugated structure of collagen previously observed.

The values of the statistical parameter "Corr" (correlation) were equipped with two distributions, both centered on higher values for the malignant node than for the benign node. In the case of the correlation ("Corr") calculated on whole SHG images, there was no significant difference between the nodules. These higher correlation values ("Corr") could indicate a regular pattern in images, which could be distinct linear fibers, present in images with malignant nodule capsules.

For small-scale images, we tested only the parameters from the fractal analysis on grayscale images ("FD-gray" and "Lac-gray" parameters). "FD-gray" values were normally distributed to the capsules of the FA and PTC nodules, with a wider distribution for the capsule of the PTC nodule, but there were no significant differences between the capsules. Therefore, "FD-gray" is more suitable for detecting changes on large-scale SHG images. On the other hand, two low components of the "Lac-gray" parameter are present in both the benign nodule capsule and the malignant nodule capsule distributions, with a higher value only for malignant nodules, consistent with the lower density of collagen fibers observed for this type of capsule. Thus, "Lac-gray" is another example of a parameter calculated on small-scale images, which could make a differentiation, while on a large scale it did not.

The Helmholtz analysis performed on small-scale images ensures only a small increase in the values of the "Helm-MedieSHG" (average) parameter of the two capsule collagen distributions studied, while the large-scale analysis returned a statistically significant increase in the parameter. "Helm-StDev" (standard deviation) for the malignant nodule capsule.

In **study no. 3**, using the same parameters of the 4 image analysis methods, we showed that there is a change in the distribution of collagen in the capsule of the malignant tumor nodule near the capsular invasion area compared to the free capsule of the thyroid nodule diagnosed histopathologically as an invasive thyroid carcinoma. In this case, eight parameters ("MedieSHG", "Hist-StDev", "Hist-Skew", "S-mean", "Contr", "Ent", "Corr" and "FD-gray") calculated from the acquired images by microscopy based on the generation of the second harmonic provided statistically significant differences between the two capsule areas investigated.

In **study no.4** we used PSHG images of thyroid tissue fragments to compare the same capsular types around PTC nodules and FA, and thyroid gland capsule. We calculated the orientation of the collagen fibers and the ratio between two non-zero elements of the second-order susceptibility tensor for collagen ($\chi 31 / \chi 15$ and $\chi 33 / \chi 15$). Attempts have been made to demonstrate that the imaging of collagen in thyroid nodule capsules at different angles of polarization of the laser beam with microscopy based on second harmonic generation describes a theoretical curve that can provide information about non-zero components of the second-order susceptibility tensor and fiber orientation of collagen. We used this approach in order to provide additional information about the collagen in the

capsule of the studied thyroid nodules, which can complete the microscopy based on the generation of the second quantitative harmonic.

Values: mode (most likely value in a data set), mean, and standard deviation resulting from a single Gaussian fit to histograms are given in Table 2.2. Mode values close to 1 are obtained for $\chi 31$ / $\chi 15$ in the case of nodular capsules, while a higher value is obtained for the thyroid capsule. Mean values are higher when matching histograms with a single Gaussian fit because the histograms are slightly inclined. No significant differences were observed in the standard deviations calculated for the three capsules. The mode values $\chi 33$ / $\chi 15$ for the thyroid capsule are significantly higher than the values for the nodule capsules, with a slightly higher value for the benign nodular capsule. Changes in $\chi 33$ / $\chi 15$ values are observed between the capsules of malignant and benign nodules. Such changes have been interpreted as possible changes in the ultrastructure of collagen fibers. An increase of $\chi 33$ / $\chi 15$ was attributed to a redistribution of fibrils and collagen fibers in the laser focal volume. Therefore, higher values of $\chi 33$ / $\chi 15$ and the standard deviation for the thyroid capsule may indicate a random organization of the capsular collagen of the benign thyroid and nodular gland and a malignant nodule capsule organized with parallel, parallel collagen fibers.

The parameter "The standard deviation" obtained for $\chi 33$ / $\chi 15$ when comparing histograms with a single Gaussian fit is larger for the thyroid capsule than for the nodular capsules, indicating a higher distribution of values, so once again greater disorganization in the distribution of collagen. The current results may seem in contradiction with those published in the literature when the values for $\chi 33$ / $\chi 15$ indicated greater disorganization of collagen fibers in the case of malignant nodules. Those results were obtained from the distribution of collagen between follicles (in the thyroid stroma) and inside the papillae in the case of thyroid papillary carcinoma, while the results of the current work are on nodular capsular collagen capsules and thyroid gland capsule, these results being consistent with those obtained for collagen fibers in nodular capsules when using SHG microscopy and texture analysis to determine the organization of collagen in the thyroid and nodular capsules.

In **study no. 5** we introduced cases of some patients diagnosed histopathologically with adenomatous multinodular goiter (benign thyroid tumor entity) in which a malignantly transformed node was incidentally discovered. We selected the cases in which, on the same section of thyroid tissue, from the same patient, we identified by conventional light microscopy the malignant nodule found among the other benign nodules. In this way we tried to eliminate the results of the recorded parameters supposed to be False-positive or False-negative, knowing that so far we have compared malignant nodules from one patient with benign nodules from another patient. We used the same method as in study no. 4 - taking into account the ratios of the elements of the susceptibility tensor (the elements in the tensor $\chi 31$, $\chi 33$, $\chi 15$ are the only non-zero values) to which we added another comparison element, namely we tried to find a way to take into account the angle resulting from the algorithm used, because the main disadvantage of the calculation methods used so far, the orientation of collagen fibers, is that they lack a reference for the angle of collagen in the case of the extracellular matrix, i.e. the orientation of collagen fiber depending on tissue orientation.

We performed a pixel-level analysis on PSHG images, aiming to identify a method for quantifying the orientation/organization of collagen fibers. By the local calculation of the scattering of the values obtained after fitting for the angle of the collagen fibers, we obtained new images on the areas on which we performed the PSHG imaging. These new images provide information on the angular scattering of collagen fibers in terms of local SD and MAD values. Using these results we identified differences between the images obtained on PTC and FA nodule capsules, respectively. At

the same time, we have shown that a combination of pixel-level analysis and image-level analysis techniques is an important method of differentiating these thyroid nodules.

5.2. Original contributions

Behind these results hides a research work, but also a consultation of the specialized literature, a re-examination of the cases from the histology of the Department of Pathology of the Central Military Emergency University Hospital for a period of 5 years (2015 - 2019), followed by a careful selection of paraffin blocks with pathological thyroid tissue suitable for the study.

We imagined and designed a complementary diagnostic procedure by extracting quantitative information regarding the orientation of collagen in thyroid tissue samples. The procedure was tested on capsules of malignant and benign thyroid nodules for their objective differentiation. We used images of the second harmonic acquired using incident laser radiation with circular polarization. The set of images was obtained from a stack of images acquired at different depths in the sample, then calculating the projection of the maximum intensity of them to obtain the final image on which the quantitative analysis was performed.

In study no. 3 we tested the ability of a first method of image analysis to differentiate the organization of collagen fibers in the 2 nodular capsular types studied. This method is the Fast Fourier Transform (FFT) analysis of SHG images for the capsule of the encapsulated papillary thyroid carcinoma and the benign nodule. In this case we found statistically significant results.

In study no. 2 quantitative analysis was performed using parameters extracted by various texture analysis methods available in an "open source" microscopy image analysis program, ImageJ. We tested the ability of these parameters to characterize the organization of collagen in images acquired by microscopy based on the generation of the second harmonic and to differentiate benign encapsulated tumors from malignant ones. This organization of collagen translates into the alignment and distribution of collagen fibers, and the set of parameters used was determined using 4 methods of textural image analysis: image histogram, "Gray Level Correlation Matrix" (GLCM) analysis, fractal analysis and Helmholtz analysis. The parameters were tested in research study no. 1 on the capsule of malignant, benign nodules and the capsule of the thyroid gland and in research study no. 2 on the capsule of the malignant tumor nodule near the area of capsular invasion and in the free capsular regions of the thyroid nodule diagnosed histopathologically as an invasive thyroid carcinoma.

Moreover, the methods used to visualize collagen in the thyroid gland capsule and thyroid tumor nodules are for the first time described on the thyroid nodule capsule in the literature, namely:

Using the image histogram, a set of four parameters, directly related to the color level distribution of pixel intensities extracted from 2D SHG images (average - "MedieSHG", standard deviation - "Hist-StDev", asymmetry index - Hist-Skew "And flattening index -" Hist-Kurt ") were calculated using the ImageJ histogram analysis toolbox. Since the intensity of SHG in each pixel depends on the density of the emitters in the focal volume, but also their organization and distribution, two additional selective parameters were considered that can be used to differentiate collagen structures that have different distributions (ratio between the number of pixels with values above a threshold and the total number of pixels - "TC-ratio" and the average value of SHG in significant areas - "S-mean"). While the mean ("MedieSHG") and the standard deviation ("Hist-StDev") are well-known statistical moments, the asymmetry index ("Hist-Skew") and the flattening index ("Hist-Kurt") describe the shape of a distribution. The pixels in the SHG image with an intensity above a threshold value are counted and the total collagen surface ratio ("TC-ratio") is determined as the ratio between

this number and the total surface area of the image. The second parameter we called the mean value of SHG in significant areas ("S-mean") is determined as the average value of the SHG signal in regions with significant SHG signals [32], using the same threshold as for the previous parameter.

A second set of parameters derived from the GLCM analysis - "Gray Level Co-occurrence Matrix" provides information about the spatial relationships between the intensities of the pixels in a given image. GLCM is constructed by adding the number of occurrences of a gray level adjacent to another gray level at a specified pixel distance - applicable especially to images that contain fibrillar structures such as SHG images of collagen and can be used to give a quantitative measurement of the mutual orientation of collagen fiber bundles. Information on the organization of collagen in SHG images can be extracted from GLCM using various parameters that have been classified in the literature as contrast, organization, and statistical parameters [33]. The contrast parameters can be used to provide quantitative information about the intensity fluctuations in the SHG image. Among these parameters, the contrast ("Contr") is a measure of the local variations present in the image, while the homogeneity or moment of the inverse difference (IDM - "Inverse Difference Moment") provides information about the similarity of a pixel value in combination with its pixel neighbor with all other pairs of neighboring pixels in the image. Organizational parameters are especially applicable to images containing fibrillar structures, such as SHG images with collagen and can be used to quantitatively measure the mutual orientation of collagen fiber bundles. For example, the energy or second angular momentum (ASM - "Angular Second Moment") is a measure of textural uniformity and reaches a maximum value equal to 1, corresponding to the highest structural uniformity, while entropy ("Ent") is a measure of the disturbance in an image. "ASM" and entropy ("Ent") are inversely correlated. Statistical parameters are based on statistical analysis of pixel value dependence and can be used to evaluate periodicity in an image. Among the statistical parameters, the correlation method ("Corr") is a strong approach applicable to SHG images with collagen fibers. We compared the correlation values ("Corr") in the GLCM analysis at different pixel distances and we matched the correlation-distance dependence (its dependence with the distance between pixels) with an exponential curve to calculate its rate of decrease.

Another method for objectively quantifying a textural organization in an image is fractal analysis. SHG images were analyzed as either grayscale or binary images. The analysis was performed using an ImageJ plugin (FracLac) that calculated the fractal size on binary images ("FD-bin"), on grayscale images ("FD-gray") and the gap on binary images ("Lac-bin"), on grayscale images using the "counting box" method. The image is covered with successive smaller boxes, and at each level are counted the boxes that contain details of the image. Such details are the white pixels in the case of binary images and the difference in pixel intensity in the area covered by the box considered for grayscale images. Fractal size [35] is a measure of image complexity, and the gap is based on the distribution of pixels in an image that is calculated from scans at different box sizes and is a measure of the depths ("pits") in an image.

Helmholtz analysis was used to determine the mean orientation distribution of collagen in SHG images. For the orientation distribution images obtained with the help of Helmholtz analysis, the same set of 4 parameters was calculated as for the 2D SHG images (mean - "Helm-MedieSHG", standard deviation - "Helm-StDev", asymmetry index - "Helm- Skew "and flattening index -" Helm-Kurt "). The values of the average parameter - "Helm-MedieSHG", were not taken into account in this case, because the average angle would depend on the orientation of the sample concerning the scan plan.

To further assess whether the differences in collagen distribution between malignant and benign capsules are due to small-scale or large-scale characteristics, all three image data sets were divided into 32x32 pixel images and all texture analysis parameters. were also calculated for these extended data sets. The obtained distributions were equipped with three Gaussian distributions for data interpretation. The quality of the fitting procedure was quantified by the coefficient of determination R^2 ($0 < R^2 < 1$), a value closer to 1 indicating a better fitting.

In study no. 3 we had another purpose, namely the early identification of the invasion area in the PTC capsule, using the same method as in the study no. 2: an extended set of 18 quantitative parameters extracted from SHG images. In this case, too, eight other parameters calculated from the images acquired by SHG microscopy provided statistically significant differences between the two investigated capsule areas, so we concluded that we could discover a certain area to be invaded in case of a possible malignant transformation of a benign nodule.

In study no.4 we used PSHG imges of thyroid tissue fragments to compare the capsules around the PTC and FA nodules with the gland capsule thyroid, so to investigate the same organization of collagen in the fibrillar capsules surrounding the thyroid nodules. Calculating the orientation of the collagen fibers and the ratio between two non-zero elements of the second order susceptibility tensor for collagen ($\chi 31 / \chi 15$ and $\chi 33 / \chi 15$) we demonstrated that the imaging of collagen in thyroid nodule capsules at different angles of polarization of the laser beam with microscopy based on the generation of the second harmonic, describes a theoretical curve that can bring information about the non-zero components of the second order susceptibility tensor and the orientation of the collagen fibers. We used this approach to provide additional information about the collagen in the capsule of the studied thyroid nodules, which can complete the SHG microscopy.

We took images on the same surface of the sample by TPEF microscopy and back-generated SHG and forward-generated SHG, respectively, and superimposed the images to have a better view of the collagen distribution in the capsules of the benign nodules of the malignant nodules and the thyroid gland capsule.

We used the same method as in study no.4, namely the ratios of the elements of the susceptibility tensor. Results were statistically relevant, except for a SHG situation collected back for $\chi 31 / \chi 15$, with the mention that $\chi 31 / \chi 15$ is a measure of anisotropy and had a lower value for the malignant nodule capsule than for the benign nodule. Then I added another element of comparison, namely I tried to find a way to take into account the angle resulting from the algorithm used, resulting in other images on which a statistical analysis can be done by calculating the pixel distribution of newly formed images. So we performed a subjective analysis of the angular distribution of collagen using pseudocolor images (depending on the pixel value) to highlight the degree of organization / disorganization of collagen fibers in capsules. On these pseudocolor images, resulting from the calculation of the angular distribution (φ) of collagen, we made another distribution of collagen orientation at the pixel level, namely we made new images of local collagen distribution, more precisely SD_l and MAD_l images with SD / MAD with compute window size with odd number of pixels l = 3, 15 and 63 pixels. At the local level there can be large variations and we noticed that at the level of the capsule of the malignant nodule the variation of pseudocolors is much more uniform. It turns out that the fibers are more aligned (more orderly). The results showed the same at the pixel level as those obtained on the entire image from previous studies, with the mention that at the pixel level we can identify exactly where the distribution of collagen fibers of the pathological nodule capsule changes.

These results suggest, for the first time in the literature, that some thyroid tumor nodules can be differentiated only by studying their capsule, without the need for tumor cell morphology, an indispensable element in developing the histopathological diagnosis of certain tumor lesions.

5.3. List of original contributions

ARTICLES IN ISI JOURNALS

1. L.G. Eftimie, R. Hristu, M. Dumitrescu, M. Costache, S.G. Stanciu, M. Sajin, G. A. Stanciu; "Modern methods to differentiate benign thyroid nodules from malignant ones"; Original Article, Romanian Journal of Military Medicine; Vol. CXXI. No.1, p.40, 2018.

2. R. Hristu, L.G. Eftimie, S.G. Stanciu, D.E. Tranca, B. Paun, M. Sajin, G.A. Stanciu; "Quantitative second harmonic generation microscopy for the structural characterization of capsular collagen in thyroid neoplasms"; Original Article, Biomedical Optics Express, vol. 9, no. 8, p. 3923, 2018.

3. Juan M. Bueno, Francisco J. Ávila, Radu Hristu, Stefan G. Stanciu, Lucian Eftimie, And George A. Stanciu"Objective analysis of collagen organization in thyroid nodule capsules using and the Hough Transform"; Applied Optics, 2020; https://doi.org/10.1364/AO.393721

4. A.M. Sîrbu, C.A. Sîrbu, L.G. Eftimie, A.M. Soare, M.C. Ghinescu, F Ioniță-Radu; "Multiple sclerosis, human herpes virus 4, and thyroid collision tumor: A case report"; Experimental and Therapeutic Medicine, 2020; https://doi.org/10.3892/etm.2020.897

5. R. Hristu, L.G. Eftimie, B. Păun, M. Costache, S.G. Stanciu, M. Sajin, G.A. Stanciu; "Pixel-level angular quantification of capsular collagen in second harmonic generation microscopy images of encapsulated thyroid nodules"; Journal of Biophotonics, 2020; https://doi.org/10.1002/jbio.202000262

NATIONAL CONFERENCES

1. L.G. Eftimie, R. Hristu, M. Dumitrescu, R.Bulata, A. Calu, M.Curea, L.Toma, F.Vasilescu, M. Costache, S.G. Stanciu, M. Sajin, G.A. Stanciu; "Tehnici moderne de diferențiere a nodulilor tiroidieni benigni de cei maligni"; Conferința Națională a Spitalului Universitar de Urgență Militar Central "Dr. Carol Davila", București, 2017 – PREMIUL 1

2. L.G. Eftimie, R. Hristu, M. Dumitrescu, R.Bulata, A. Calu, M.Curea, L.Toma, F.Vasilescu, M. Costache, S.G. Stanciu, M. Sajin, G.A. Stanciu; "Microscopia bazată pe generarea armonicii a doua (SHG) poate ajuta patologul în a diagnostica Carcinomului papilar tiroidian, prin identificarea invaziei capsulare?"; Conferința Națională a Spitalului Universitar de Urgență Militar Central "Dr. Carol Davila", București, 2018.

3. L.G. Eftimie, R. Hristu, M. Dumitrescu, R.Bulata, A. Calu, M.Curea, L.Toma, F.Vasilescu, R. Glogojeanu, M. Costache, S.G. Stanciu, M. Sajin, G.A. Stanciu; "Corelații între microfotografii pe secțiuni colorate cu H&E și imagini de microscopie multifotonică achiziționate pe nodulii încapsulați tiroidieni"; Conferința Națională a Spitalului Universitar de Urgență Militar Central "Dr. Carol Davila", București, 2019.

INTERNATIONAL CONGRESSES - ABSTRACTS APPEAR IN ISI PROCEEDINGS

1. L.G. Eftimie, R. Hristu, O. Voinea, M. Dumitrescu, M. Sajin, G.A. Stanciu; "Differential diagnosis between benign and malignant thyroid nodules using Second Harmonic Generation Microscopy"; Poster European Congress of Pathology, Amsterdam, 2017.

2.   L.G. Eftimie, R. Hristu, M. Dumitrescu, M. Costache, S.G. Stanciu, M. Sajin, G.A. Stanciu; "Modern methods for the structural characterization of collagen in capsular invasion areas in papillary thyroid carcinoma"; Poster European Congress of Pathology, Bilbao, 2018.

3.   R. Hristu, B. Paun, L.G. Eftimie, S.G. Stanciu, D.E. Tranca, G.A. Stanciu; "Changes in the Collagen Structure of Thyroid Nodule Capsules Determined by Polarization-Resolved Second Harmonic Generation Microscopy", ICTON (20th International Conference on Transparent Optical Networks), București, 2018.

4. R. Hristu, L.G. Eftimie, G.A. Stanciu; "Second harmonic generation imaging for materials science and biomedical applications", 2020 2nd International Conference on Advanced Materials and Ecological Environment, 2020

5.4. Future development perspectives

Given the results presented in this thesis, I believe that it could have practical application in the medical field, because it would fall into the category of complementary methods, helping to develop a histopathological diagnosis as accurate as possible. Used as an additional technique with applicability in Pathological Anatomy could help to avoid underdiagnosis or overdiagnosis of lesions, whose correct diagnosis is essential for proper and effective treatment. Also, by using this technique, it will be avoided to use more than other relatively expensive complementary diagnostic techniques currently existing (molecular biology techniques, genetic tests, IHC tests, electron microscopy, etc.).

The hypothesis of another bold applicability could be raised, which would revolutionize the medical world if a small device with the properties of laser scanning microscopy based on the generation of second harmonics (SHG) were built, which can be easily manipulated by the examining physician on anterior cervical region. Thus, images with pathological thyroid nodules can be viewed transtegumentarily "in vivo", using live software implemented with the methods presented by capsular textural analysis, using the parameters used in this paper, which could generate a "correlation graph - regression line" on benign or malignant tumor capsular character. This method could compete with ultrasonography, as a noninvasive, non-traumatic imaging method for exploration and diagnosis for superficially located organs, such as the thyroid gland. It can also successfully replace the technique of biopsy for histopathological diagnosis or fine needle aspiration under ultrasonographic guidance to take cellular material for a cytopathological diagnosis, minimally invasive methods currently used to confirm the malignancy of a thyroid nodule and establish surgical indication.

At the moment, the method has limitations in terms of costs, training of medical staff in using it, large dimensions of the equipment and would be worth implementing if it would extend its medical applicability to other encapsulated lesions. At the same time, research will be needed on a much larger group of patients and clinical trials for the method to be validated by the Ministry of Health.

Selective Bibliography

[1]   World   Health   Organization   [https://www.who.int/en/news-room/fact-sheets/detail/cancer]

[2]   American Cancer Society [https://www.cancer.org/cancer/thyroid-cancer/about/key-statistics.html]

[3]   Larsen, William J. (2001). Human embryology (3. ed.). Philadelphia, Pa.: Churchill Livingstone. pp. 372–374. ISBN 978-0-443-06583-5.

[4]   S. E. Mills, Histology For Pathologists. Fourth Edition., Md. 2012, 2007 By Lippincott Williams & Wilkins, A Wolters Kluwer Business. Isbn 978-1-4511-1303-7.

[5]   R. V. Lloyd, R. Y. Osamura, G. Kloppel, J. Rosai, WHO Classification of tumours of endocrine organs, 4th edition, International Agency for Research on Cancer, Lyon, 2017, p.65-96.

[6]   J. Rosai, R. A. DeLellis, M.L. Carcangiu, W.J Frable, G. Tallini; AFIP Atlas Of Tumor Pathology. Tumors Of The Thyroid And Parathyroid Glands. Fourth Series. Fascicle 21. American Registry Of Pathology. Silver Spring, Maryland, 2014.

[7]   P. Davidovits and M. D. Egger, Photomicrography of Corneal Endothelial Cells in vivo, Nature, 244: 366-367, 1973.

[8]   J. M. Bueno, F. J. Ávila, and P. Artal, "Second Harmonic Generation Microscopy: A Tool for Quantitative Analysis of Tissues," in Microscopy and Analysis, S. G. Stanciu, Ed. InTech, 2016.

[9]   E. A. Gibson, O. Masihzadeh, T. C. Lei, D. A. Ammar, and M. Y. Kahook, "Multiphoton microscopy for ophthalmic imaging," Journal of Ophthalmology, vol. 2011, pp. 1–11, 2011, doi: 10.1155/2011/870879.

[10]   Cicchi, Riccardo; Vogler, Nadine; Kapsokalyvas, Dimitrios; Dietzek, Benjamin; Popp, Jürgen; Pavone, Francesco Saverio (2013). "From molecular structure to tissue architecture: collagen organization probed by SHG microscopy". Journal of Biophotonics. 6 (2): 129–142. doi:10.1002/jbio.201200092. ISSN 1864-063X

[11]   I. Amat-Roldan, et. al.: Fast image analysis in polarization SHG microscopy, Opt. Express, vol. 18. pp.17209-17219, 2010.

[12]   J. Adur et al., "Second harmonic generation microscopy as a powerful diagnostic imaging modality for human ovarian cancer," J. Biophotonics, 2014.

[13]   Z. fang Li, S. ping Qiu, S. lian Wu, and H. Li, "Quantification of collagen fiber orientation based on center line of second harmonic generation image for naturally aging skins," Optoelectron. Lett., 2018.

[14]   A. Golaraei et al., "Polarimetric second-harmonic generation microscopy of the hierarchical structure of collagen in stage I-III non-small cell lung carcinoma," Biomed. Opt. Express, 2020.

[15]   L. B. Mostaço-Guidolin et al., "Collagen morphology and texture analysis: From statistics to classification," Sci. Rep., 2013.

[16]   K. E. Frisch, S. E. Duenwald-Kuehl, H. Kobayashi, C. S. Chamberlain, R. S. Lakes, and R. Vanderby, "Quantification of collagen organization using fractal dimensions and Fourier transforms," Acta Histochem., 2012.

[17] K. Tilbury, J. Hocker, B. L. Wen, N. Sandbo, V. Singh, and P. J. Campagnola, "Second harmonic generation microscopy analysis of extracellular matrix changes in human idiopathic pulmonary fibrosis," J. Biomed. Opt., 2014.

[18] C. Bayan, J. M. Levitt, E. Miller, D. Kaplan, and I. Georgakoudi, "Fully automated, quantitative, noninvasive assessment of collagen fiber content and organization in thick collagen gels," J. Appl. Phys., 2009.

[19] X. Chen, O. Nadiarynkh, S. Plotnikov, and P. J. Campagnola, "Second harmonic generation microscopy for quantitative analysis of collagen fibrillar structure," Nat. Protoc., vol. 7, no. 4, pp. 654–669, 2012.

[20] D. Tokarz, R. Cisek, A. Golaraei, S. L. Asa, V. Barzda, and B. C. Wilson, "Ultrastructural features of collagen in thyroid carcinoma tissue observed by polarization second harmonic generation microscopy," Biomed. Opt. Express, 2015.

[21] N. Mazumder, J. Qiu, M. R. Foreman, C. M. Romero, P. Török, and F.-J. Kao, "Stokes vector based polarization resolved second harmonic microscopy of starch granules," Biomed. Opt. Express, 2013.

[22] S. Psilodimitrakopoulos, S. I. C. O. Santos, I. Amat-Roldan, A. K. N. Thayil, D. Artigas, and P. Loza-Alvarez, "In vivo, pixel-resolution mapping of thick filaments' orientation in nonfibrilar muscle using polarization-sensitive second harmonic generation microscopy.," J. Biomed. Opt., 2011.

[23] J. Duboisset, D. Aït-Belkacem, M. Roche, H. Rigneault, and S. Brasselet, "Generic model of the molecular orientational distribution probed by polarization-resolved second-harmonic generation," Phys. Rev. A - At. Mol. Opt. Phys., 2012.

[24] I. Amat-Roldan, S. Psilodimitrakopoulos, P. Loza-Alvarez, and D. Artigas, "Fast image analysis in polarization SHG microscopy," Opt. Express, 2010.

[25] B. Paun, R. Hristu, S. G. Stanciu, A. V. Dumitru, M. Costache, and G. A. Stanciu, "Strategies for Optimizing the Determination of Second-Order Nonlinear Susceptibility Tensor Coefficients for Collagen in Histological Samples," IEEE Access, 2019.

[26] P. Réfrégier, M. Roche, and S. Brasselet, "Precision analysis in polarization-resolved second harmonic generation microscopy," Opt. Lett., 2011.